Polarized random fibre lasers based on the tilted fibre Bragg grating

Xiaojuan Zhang

MSc by Research

Aston University

July 2019

Aston University

Polarized random fibre lasers based on the tilted fibre Bragg grating

Xiaojuan Zhang

MSc by Research

July 2019

In the traditional random fibre lasers (RFLs), it is complicated to generate polarized random fibre lasing. In this thesis, I present a new method to obtain polarized random fibre lasers (RFLs). In my research, 45° tilted fibre Bragg grating (45° TFG) fabricated in single mode fibre (SMF) or in Erbium doped fibre (EDF) has been integrated with the fibre laser and the polarized random lasing was achieved using 45° TFG with high polarization extinction ratio (PER) characteristics.

In this thesis, first of all, I present the review of random lasers (RLs), random fibre lasers (RFLs), and corresponding polarization characteristics. And then I present a detailed research work on the method, characteristics and applications of fibre gratings, including fibre Bragg gratings (FBGs), long period gratings (LPGs), and TFG with small and 45° tilted structures.

One of the major contributions of my work in this thesis is the investigation on phase-match conditions, transmission spectra, PER for different types of fibre gratings including the TFG, FBG, and LPG. The results show that 45° TFG has high PER with 14 dB and the 7° TFG has comb-like resonance transmission. And then I present the experimental research of the thermal sensing of different types of fibre grating. LPG with grating period of 480 μm has the highest thermal sensitivity with 297.1 pm/°C, superior to the FBG, small angle TFG and LPG. Meanwhile, I also researched the strain sensing application of FBG. The strain sensitivity of the FBG is 0.71±0.01 pm/°C.

The other important contribution from the work is that I researched the polarization random fibre lasing feature with 45° TFG in the two fibre laser systems, which are Raman distributed SMF system and EDF with Raman distributed SMF hybrid system. In the Raman distributed SMF with length of 20.1 km system, there are three kinds of emission spectra with the increase of pump power from 1.70 W to 3.00 W: Raman emission, non-stationary random lasing emission, and stationary random lasing emission. The random lasing threshold is measured as 2.10 W. When the 45°TFG is added in the system, the polarized random lasing with PER of 12.02 dB has been obtained. In the EDF (2 m length) and Raman distributed SMF (11 km length) hybrid system without 45° TFG, there are two kinds of emission with the increase of pump power from 2.60 W to 4.40 W: Raman emission, and non-stationary random lasing. The stationary random lasing has not been observed due to the pump power limit. When the 45° TFG has been integrated in the hybrid system, we observed two kinds of emission in a range of pump power of 1.00 W to 2.20 W: Raman and Er^{3+} emission, and stationary random lasing. Under the effect of weak cavity formed by 45° TFG reflection and SMF distributed feedback, there occurs stabilized random fibre lasing emission. The threshold has been determined as 1.44 W. In addition, under the effect of 45° TFG, the polarized random fibre lasing with PER of 15.3 dB has been obtained.

Key words: Random fibre lasers, Fibre Bragg grating, Long-period grating, Tilted fibre grating, Polarization.

To my son Andi Hu.

Acknowledgements

Contents

ACRONYMS

RL	Random laser
RFL	Random fibre laser
TFG	Tilted fibre Bragg grating
PER	Polarization extinction ratio
FBG	Fibre Bragg grating
LPG	Long period of grating
FWHM	Full width at half maximum
POF	Polymer optical fibre
TM	Transverse magnetic
TE	Transverse electric
NLC	Nematic liquid crystal
PDLC	Polymer-dispersed liquid crystal
SMF	Single mode fibre
MMF	Multiple mode fibre
SOP	State of polarization
PM	Polarization maintaining
Ge	Germanium
GDF	Graphene-coated D-shaped fibre
PR	Polarization rotator
LR	Long-range

SR   Short-range

ns   nano-second

Eu   Europium

Ce   Cerium

Er   Erbium

Al_2O_3 Aluminium oxide

BBS   Broadband light source

FG   Fibre grating

P   Polarizer

PC   Polarization controller

OSA   Optical spectrum analyser

TS   Translation stage

EDF   Erbium doped fibre

List of figures

11

Chapter 1. Introduction and Thesis Structure

1.1 Introduction

Since V. S. Letokhov theoretically proposed random lasers (RLs) [1-2], it has been widely researched in different system [3-8]. RLs are the stimulated emission from gain scattering system, which do not need the resonant cavity to feedback light. The feedback mechanism depends on the multi-scattering feedback [9]. Until 1990s, N. M. Lawandy's group [5] and H. Cao's group [3, 10] respectively found the incoherent RLs and coherent RLs in the experiments, which greatly promote the development of RLs. Later, RLs were found in the different disorder systems including gain medium with scattering particles and gained scattering particles [11-12]. The RLs have several advantages features, *e.g.*, low spatial coherence and high photon degeneracy, small size, easy to integrate [13]. However, for the simplification of light feedback reason, there are some disadvantages including high threshold, non-directivity and hard controlling the random lasing emission. To solve the high threshold and non-directivity, C. J. S. de Matos used the photonic crystal fibre to confine the random lasing system, which promote the birth of random fibre laser (RFL) [14]. After this report, many other kinds RFLs were researched [15-19]. However, it is also not easy to control the random lasing emission for RFLs including wavelength and polarization.

To get polarized PFLs, there mainly are two ways to control polarization including induces anisotropic factors and polarization elements in the RFLs system [20-21]. From the application perspective of RFLs, the silica distributed RFLs is an important candidate, which can be applied in the optical communication, laser display, optical sensors, and speckle-free laser source [22]. It is not convenient to obtain polarized RFLs whether inducing anisotropic factors and polarization elements in the fibre system. Therefore, we will research a new simple way to obtain polarized RFLs.

In 2005, K. Zhou *et. al.* fabricated 45°-tilted fibre Bragg grating (45°-TFG) as a polarizer in a standard single mode fibre (SMF) [23]. Compare with the traditional polarization elements, the 45°-TFG has significant advantages, *e.g.*, low-cost, effective and all fibre system. In principle, the TE light transmitting through 45°-TFG has large transmission loss whereas the TM-light has small loss due to Brewster's Law. Therefore, I will integrate the 45°-TFG in the SMF system to obtain high PER

polarization Raman fibre RLs. This simple, low-cost, effective and all fibre polarization RFLs will extend the application of RFL.

1.2 Structure of thesis

The thesis consists of five chapters; the detailed contents for each chapter are listed below:

Chapter 1 provides a brief introduction on random lasing development and the motivation for my Master's research work, and then describes the structure of the thesis.

Chapter 2 will begin with a review of RLs and RFLs. Subsequently, the polarized RLs and RFLs are introduced. As the second major part of this chapter, we first introduce the development of optical fibre gratings. Second, we review the mechanism photosensitivity of optical fibre in details. Finally, the theory of the mode coupling mechanisms for fibre grating is discussed systematically.

Chapter 3 presents the measurement the characteristics including transmission spectra and polarization extinction ratio (PER) for different types of fibre grating of fibre Bragg grating (FBG), long period of grating (LPG), and TFG. Furthermore, the stress sensors of FBGs and temperature sensors of LPGs and TFGs are researched.

Chapter 4 reports the polarized random fibre lasing emission based on Raman gain by adding the 45°-TBG in the SMF system.

Chapter 5 presents the thesis conclusions and gives some detailed suggestions for future research works.

Chapter 2. Background Review (History, Photosensitivity, Grating Theory, Fabrication Methods, and Random Fibre Lasers)

2.1 Random laser and random fibre laser

2.1.1 Random lasers history

Since V. S. Letokhov theoretically proposed random lasers (RLs) in 1967, it has been widely researched in different system [1, 24, 25]. RLs are different from the traditional lasers, which do not need the resonant cavity, *e.g.*, several mirrors, to feedback light in the cavity [26]. Figure 2.1 shows the different feedback mechanism for RLs and traditional lasers. RLs can be realized in the disorder gain system [27]. The light multi scattering caused by the disorder scatter, *e.g.*, nanoparticles [28-30], material density fluctuation [31], phase non-uniformity [32-34] and porous structure [35-37], provides analogous feedback cavities, which boost the light amplification. When the gain is larger than loss, there occurs stimulated lasing emission. The RLs can be obtained in different system, *e.g.*, nanoparticles and dyes [38, 39], liquid crystals and dyes [40, 41], gain polymer [42, 43]. Based on the feedback mechanism, the RLs can be divided into two different regimes [9]: 1) *incoherent RLs* with intensity and energy feedback, 2) *coherent RL* with field and amplitude feedback.

Aston University

Illustration removed for copyright restrictions

Figure 2.1 Two different feedback mechanisms for traditional lasers and RLs [27].

In 1994, N. M. Lawandy *et. al.* first experimentally observed the similar lasing emission in the methanol colloidal suspension solution with laser dye and TiO_2 nanoparticles, as shown in the Figure 2.2 [5]. When the pump energy is over the threshold, the full width at half maximum (FWHM) of emission spectra narrows to 4 nm from 70 nm. Scientists speculate that there is resonant cavity to feedback the light in the random gain system to cause the narrow effect. In addition, there is not light coherence effect to generate the spike peaks emission (<1 nm) in these spectra. Therefore, we called these lasing emissions as incoherent RLs in the disorder gain system. Later, D. S. Wiersma and A. Lagendijk [4]

use the light diffusion theory to explain the multi-scattering causing incoherent RLs phenomenon.

Aston University
Illustration removed for copyright restrictions

Figure 2.2(a) The emission spectrum of Rhodamine 640 perchlorate dye solution with 2.5×10^{-3} M in methanol at pump energy of 3 mJ; (b) and (c) emission spectrum of TiO_2 nanoparticles (2.8×10^{10} cm^{-3}) colloidal dye solution at pump energy of 2.2μJ and 3 mJ, respectively. The intensity of the spectrum of b (c) has been scaled up (down) by a factor of 10 (20) [14].

In the 1998, H. Cao *et. al.* reported the spike and independent lasing emission (<1 nm) in the ZnO powder and poly-crystal film using nanosecond pump laser [10] when the pump energy increases over the threshold. In different collection direction and time, the lasing emission spectra is completely different. That is why this kind of lasing emission is called as ***random lasing***. S. V. Frolov [6, 7] R. C. Polson [8] and K. Yoshino [44] have research the coherence RLs in the pi-copolymer films, colloidal film with dye and dye permeated crystal materials. This spike lasing phenomenon are essential different from the incoherent RLs. There should be a resonant cavity in the disorder gain system to get a series of independent lasing peaks, which are similar with the longitudinal modes of traditional lasers. Thus, these kinds of lasers are called coherent RLs.

Figure 2.3 The emission spectra for the zinc oxide polycrystalline films with different pump area at the excitation intensity of 400 kW/cm^2: (a) 2700 μm^2, (b) 3800 μm^2, and (c) 4500 μm^2. The inset: the schematic diagram for the formation of a closed-loop path of multiple light optical scattering in a random medium [10].

Due to lack of the resonant feedback, the RLs have several advantages features: 1) low spatial coherence and high photon degeneracy, it can be as light sources in the speckle-free full-field imaging; 2) small size due to simply the cavity structure, it can be realized in the micro-nano device; 3) easy to integrate in the silica fibre or polymer fibre as sensors. Meanwhile, for this simplified resonant cavity reason, the RLs also has some disadvantages: 1) *high threshold*; 2) *non-direction*; and 3) *random lasing wavelength*.

2.1.2 Random fibre lasers (RFLs) history

2.1.2.1 Regime of random fibre lasers

To preferably understand the history of RFLs, I summarize different kinds of RFLs, as shown in the Figure 2.4. Here, I introduce three kinds of random fibre lasers (RFL) from materials point of view.

```
                              ┌─────────┐
                              │  RFLs   │
                              └─────────┘

   In active fibres                                    In passive fibres
┌──────────────────────────────┐          ┌──────────────────────────────┐
│ RFLs based on stimulated      │          │ RFLs based on stimulated      │
│ emission                      │          │ scattering                    │
└──────────────────────────────┘          └──────────────────────────────┘

┌──────────────┐  ┌──────────────┐  ┌──────────────┐  ┌──────────────┐
│ Liquid core  │  │ "Scatter+gain"│  │ Stimulated   │  │ Stimulated   │
│ RFLs based on│  │ or "gained    │  │ Raman        │  │ Brillouin    │
│ "scatter+gain"│ │ scatter"      │  │ scattering   │  │ scattering   │
│ or "gained   │  │ material doped│  │ based RFLs in│  │ based RFLs in│
│ scatter"     │  │ POFs or silica│  │ silica fibres│  │ silica fibres│
│ material     │  │ fibres        │  │ and POFs     │  │              │
│ filled hollow│  │               │  │              │  │              │
│ optical fibres│ │               │  │              │  │              │
└──────────────┘  └──────────────┘  └──────────────┘  └──────────────┘
```

Figure 2.4 Different kinds of RFLs.

➢ **Liquid core RFLs**

To solve these weakness points of RLs, C. J. S. de Matos first investigated the effects of 2-dimensinal confinement on the random lasing of disorder scattering system [14]. The Rhodamine 6G and TiO_2 nanoparticles with 250 nm suspension solution was filled into the hollow core of photonic crystal fibre, bringing the birth of incoherent RFL by side pump, as shown in the Figure. 2.5. The laser efficiency of RFL is about two orders of magnitude higher than that of bulk format (see Figure 2.6).

Aston University
Illustration removed for copyright restrictions

Figure 2.5 Side view of the experimental setup. VNDF: Variable neutral density filter; CL: Cylindrical lens; SH: Sample holder; SL: Spherical lens; SPEC: Spectrometer. Inset: Scanning electron microscopy of the photonic crystal fibre [14].

Figure 2.6 The emission spectra for different pump power density and configurations: (a) Rh 6G (10^{-4} M) and rutile particles (10^8 cm^{-3}) in the ethyleneglycol solution in a cell; (b) Rh 6G (10^{-4} M) in ethylene glycol inside the photonic crystal fibre without scattering particles; (c) Rh 6G (10^{-4} M) in ethylene glycol inside the photonic crystal fibre with rutile particles (10^8 cm^{-3}) [14].

Figure 2.7 The emission spectra of PM597/POSS nanoparticles in CS$_2$ solutions at different pump energies in (a) the cuvette and (b) liquid core fibre system; (c) Dependence of the main-peak intensities (solid symbols) as well as the integrated emission intensities (open symbols) on the pump energies, with circles and triangles for (a) and (b), respectively; (d) the experimental setup [16].

In the 2012, Z. Hu *et. al.* reported coherent RFL in the POSS and PM597 laser dye filled hollow optical fibre [16]. In addition, they proved that the waveguide effect enhances the multiple scattering intensity in the hollow optical fibre. They also researched the localized surface plasmon resonance of gold nanoparticles enhancing the random lasing emission in the liquid core fibre [45].

> **Silica RFLs**

To extend the application of RFLs, S. K. Turitsyn *et. al.* obtained distributed feedback RFLs based on *the **Rayleigh scattering** and **amplified Raman gain*** in the traditional silica single mode communication fibre [18]. These RFLs are different from the traditional fibre lasers with resonant cavity in the spatial coherence. But the RFLs also have the same features with traditional fibre lasers, *e.g.*, narrow emission and Gaussian light beam. X. Bao *et. al.* researched the other kinds of distributed RFLs based on the ***Rayleigh scattering** and **amplified Brillouin gain*** in the SMF [46]. These kinds of RFLs can be realized easily, which will be applied in the optical communication, speckle-free full-field imaging and sensors. R. Ma *et. al.* successfully realized multimode RFLs are as an effective light source in speckle-free imaging using its low spatial coherence [22]. This work will pave a way to future research RFL application in the optical fibre imaging.

Figure 2.8 The different feedback and gain mechanisms of silica RFLs: (a) Raman RFLs [18] and Brillouin RFLs [19].

The fibre length required for random lasing can be determined based on the random distributed Raman scattering feedback as follows [18].The fibre longitudinal distribution of Raman gain $g_R P_{\mathrm{p}}(z)$ can be estimated by the pump power attenuation neglecting pump depletion due to Stokes light generation:

$$P_{\mathrm{p}}(z) = P_0 \exp[-\alpha_p |z|], \qquad (2.1)$$

where α_p is the pump light loss coefficient with 0.057 km^{-1}, P$_0$ is the input pump power, z is the fibre distance, and $z = 0$ is two pump waves with 1455 nm coupled point as shown in the Figure 2.8 (a). Based on the gain and loss balance condition, the length of the amplification region $2L_{RS}$ can be estimated by

$$g_R P_p(L_{RS}) = \alpha, \tag{2.2}$$

giving
$$L_{RS} = \ln(g_R P_0 / \alpha) / \alpha_p, \tag{2.3}$$

where g_R is the Raman gain coefficient, α is the loss coefficient of optical fibre. Therefore, the optical fibre length used in the experiment $L \approx 2L_{RS}$, ensures random lasing caused by random distributed feedback. When the optical fibre length increases to more than $2L_{RS}$, the length has little influence on random lasing. The random lasing threshold will be slightly decrease due to the attenuation of the lasing when $|z| > L_{RS}$. Meanwhile, the lasing intensity will be exponential decayed because of the attenuation in this region.

Taking consideration of average Rayleigh backscattering coefficient ε, the more detailed theoretical description lasing power evolution can be given by

$$\frac{dP^\pm(z)}{dz} = \mp\alpha P^\pm(z) \pm g_R(P_p^+ + P_p^-)P^\pm \pm \varepsilon P^\mp, \tag{2.4}$$

where $P^\pm(z)$ are the generated Stokes waves light and $P_p^\pm$ are the pumping light, with $\pm$ corresponding to forward and backward propagation, respectively. In the numerical simulations, the more accurate model should consider other factors including spontaneous emission, attenuation, power depletion and backscattering for both pumping and generated lasing waves.

Based on the integral gain and loss balance equation at the 'roundtrip' process within an optical fibre with the effective 'distributed mirror', provide by the Rayleigh backscattering, the lasing threshold condition can be defined by

$$\varepsilon \int_0^{L/2} dz \exp[-2\alpha z + 2g_R \int_0^z P_p(s)ds] = 1. \tag{2.5}$$

We can obtain an analytic expression for the lasing threshold for $L >> 2L_{RS}$ using a standard saddle point approximation as

$$P_0 = \frac{\alpha}{g_R}(1 + \ln(\frac{g_R P_{th}}{\alpha})) + \frac{\alpha_p}{2g_R}\ln(\frac{1}{\varepsilon}\sqrt{\frac{\alpha\alpha_P}{\pi}}).$$

(2.6)

Therefore, we can calculate numerically the lasing threshold pump power with Raman feedback $P_{th}^{RS} = 2P_0$ for different optical fibre length.

➤ **Polymer RFLs**

Compare with silica fibre, polymer optical fibres (POFs) have unique characters, *e.g.*, flexibility, low cost, large numerical aperture, and ease of handing. They have been researched in the fibre lasers [47], amplifiers [48], sensors [49], and wearable phototherapy devices [50]. In 2013, Z. Hu *et. al.* reported the coherent RFLs in the POSS nanoparticles doped gain POFs [17]. The threshold of the polymer RFL is about one order of magnitude lower than that of liquid core fibre RLs [15]. Meanwhile, the random lasing wavelength can be stabilized, which can be attributed to the Anderson light localization in the POFs [51]. In addition, they controlled the random lasing wavelength emission by thermal effect due to polymer with high thermo-optical coefficient. The random lasing wavelength tunable range is about 17 nm [52]. In 2018, J. He *et. al.* simulated the random lasing dynamics using a four-level Monte Carlo model in the one-dimensional POF and open the speckle-free imaging research [53].

Aston University
Illustration removed for copyright restrictions

Figure 2.9 The polymer fibre random laser; (a) materials chemical structures; (b) the optical microscope cross-sectional image of the disorder POF with POSS nanoparticles; (c) schematic of POF system with random lasing; (d), (e) the TEM images of POSS nanoparticles at different scale bars in the core of the disorder POF [17].

2.1.3 Polarized random fibre lasers

2.1.3.1 Polarized random lasers

The polarization emission is very important for the lasers' application. While, the polarization emission for lasers can be controlled by polarization elements such as Lyot filters or Brewster windows. However, the RLs systems lack of the resonant cavity and polarization elements, which lead in non-polarized random lasing emission in the traditional disorder gain system. Therefore, anisotropic materials or structures have been designed to control the polarization of RLs. There are three ways to obtain polarized random lasing in the disorder gain system.

➢ **Anisotropic absorption**

For the anisotropic dye, the molecule's transition momenta force the polarization of lasing emission close to the pump liner polarization. S. Knitter *et. al.* presented a polarized random lasing in the asymmetric dye under the linear polarization pump [54]. L. Ye *et. al.* used the oriented polymer chain to shear the alignment direction of liquid crystal and laser dye [55]. Thus, the anisotropic absorption for the dye can boost the polarization lasing emission. It is not easy to synthesize asymmetric laser dye or obtain anisotropic alignment dye. Therefore, this way is not a main way to control the polarization of random lasing emission.

➢ **Anisotropic scattering**

Based on the electromagnetic theory, the zero-forward and zero-backward scattering intensity can be controlled through anisotropic permittivities in the anisotropic nanoparticles scattering [56]. J. Liu *et. al.* simulated the polarization-dependent random lasing emission by using Maxwell's equations and electronic population rate equations in two-dimensional gain disorder media for both transverse magnetic (TM) and transverse electric (TE) fields [57]. Based on the liquid crystals anisotropic scattering, F. Yao *et. al.* presented the polarized random lasing research in the dye doped nematic liquid crystals (NLCs) [58]. They obtained the linear polarized random lasing, and the polarization direction is close to the bisection between the maximal scattering direction in NLCs and the nematic director. And the random lasing polarization can be changed by rating the NLCs sample direction. S. Xiao *et. al.* obtained the switch polarization RL in the dye doped polymer-dispersed liquid crystal (PDLC) film [59]. The polarization state of random lasing is changed to only *p* polarization when the electric field of 9.2 V/μm is applied in the PDLC film. This PDLC polarized random lasing source can be used in

the display areas and integrated in the optical devices. The ***anisotropic structures*** can also exploit polarization random lasing. E. S. P. Leong *et. al.* demonstrated TE random lasing emission for anisotropic ZnO rib waveguide due to TE mode with large confinement factor and scattering strength inside the random scatter rib waveguide [60].

2.1.4 Polarized random fibre lasers

2.1.4.1 Liquid core RFLs

In this kind of RFLs, the nanoparticles and laser dyes dopant are isotropous [14, 16]. It is impossible to generate the polarized random lasing emission. Because this kind of liquid core optical fibres is not standard SMF or multiple mode fibre (MMF) it cannot be integrated with fibre polarization elements easily. Therefore, there is not appear to report polarized random lasing in the liquid core RFLs.

2.1.4.2 Silica RFLs

Based on the gain mechanism, silica RFLs can be divided into two regimes: Raman RFLs and Brillouin RFLs. In these kinds of RFLs, it is hard to obtain the polarized random lasing emission based on Rayleigh scattering feedback because the local birefringence along SMF is strongly disturbed by external perturbations, which leads to the deterioration of the polarization of RLs characteristics. Therefore, to obtain polarized RFL it should add polarization elements or induce anisotropic structure in the fibre system.

➢ **Polarized Raman RFLs**

Under the non-polarization laser pumping the traditional SMF, there is only non-polarization random lasing emission. H. Wu *et. al.* tried to obtain the partially polarized random lasing emission utilizing polarized pump and non-polarization-maintaining fibre [61]. The state of polarization (SOP) of random lasing emission changes with the SOP of pumping laser. X. Du *et. al.* realized linear polarization lasing output using 0.5 km length polarization maintaining (PM) fibre and high reflectivity PM fibre Bragg grating in the half-opened cavity using depolarized pumping [62]. The PM fibre provides Raman gain and random distributed feedback. In addition, they taken the fibre coiling technique to suppress high-order modes and utilized the different blend loss between the fast and slow axis polarization modes, realizing polarization extinction ratio (PER) >14 dB at pump power of ∼3W. E. A. Zlobina *et. al.* further

optimized the experimental setup to obtain linear polarization random lasing with PER >25 dB in all range of obtained powers (<9.4 W) using an all-PM configuration [63]. J. Xu *et. al.* also obtained linear seed random lasing with PER of 22.5 dB in the half-opened cavity including a linearly polarized narrow-linewidth FBG and a 500 m piece of polarization-maintained germanium (Ge)-doped fibre [64]. Later, J. Ye *et. al.* obtained high power linearly polarized RFL of 23 W with PER > 20 dB in the 1102.5-1112.5 nm and researched its flexible spectral manipulation property [65]. Using a bandwidth-adjustable tunable optical filter, the central wavelength can be controlled from 1095 to 1115 nm and FWHM linewidth from 0.6 to 2 nm. Meanwhile, they also researched the linear polarized random lasing property of power scaling capability using Lyot filter into a half-opened RFL system.

Figure 2.10 The polarized RFLs experimental setup: PM coupler: polarization-maintaining fused fibre coupler, PM FWDM: polarization maintaining filtered wavelength-division multiplexer, OSA: optical spectrum analyzer, L: lens, A: broadband attenuator, P: Glan–Thompson polarizer [63].

In 2015, B. Yao *et. al.* adopted graphene-coated D-shaped fibre (GDF) to obtain polarized random lasing in the half-opened cavity with 50 km SMF via a polarization rotator (PR) [66]. Due to the graphene's anisotropy, the loss of the TM polarization light is much larger than that of TE polarization in the GDF. Therefore, the GDF and PR co-work to generate linear polarized random lasing with PER of 41 dB.

➤ **Polarized Brillouin RFLs**

In the silica RFLs, there is the other kind of RFLs-Brillouin RFLs- based on the Brillouin gain and the Rayleigh scattering. In the experiences to obtain linear Raman RFLs, the way utilizing PM fibre as gain medium and Rayleigh scattering medium can also be applicative in the polarized Brillouin RFLs. L. Zhang *et. al.* obtained linear polarized Brillouin RFLs with PER of >25 dB in the 2 km PM fibre using linear pumping [67]. In addition, they have reported high-efficiency linear Brillouin RFLs in the later work [68].
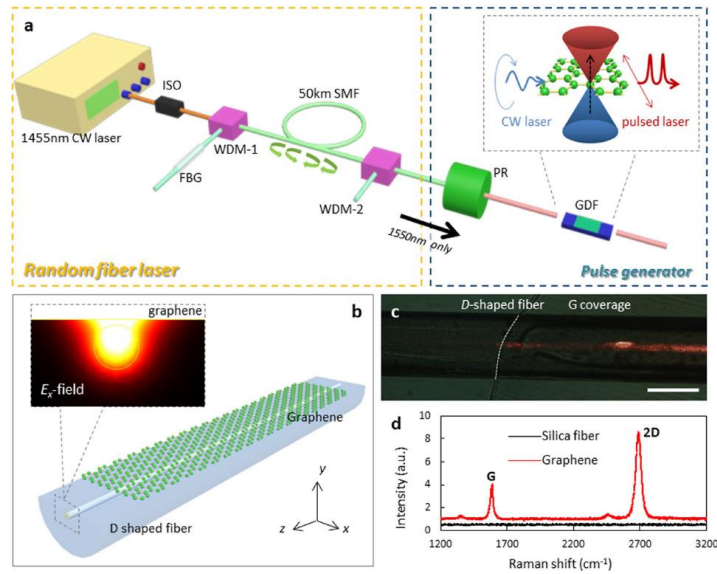
Figure 2.11 The polarized RFLs experimental setup: PM coupler: polarization-maintaining fused fibre coupler, PM FWDM: polarization maintaining filtered wavelength-division multiplexer, OSA: optical spectrum analyzer, L: lens, A: broadband attenuator, P: Glan–Thompson polarizer [66].

Figure 2.12 The polarized random lasing from disorder POFs [69].

2.1.4.3 Polymer RFLs

Anisotropic element is key role to generate polarized random lasing. And polymer is a king of soft matter, which can be easily modified to as anisotropic material. In the 2016, Z. Hu *et. al.* demonstrated a polarized RFL in the different oriented disorder gain POF based on anisotropic scattering [69]. First, they controlled and fabricated different kinds of oriented POFs, *e.g.*, PM597 laser dye doped POF (long-range disorder POF, called LR disorder POF), POSS nanoparticles and PM597 doped POF (short-range POF, called SR disorder POF) and Au nanoparticles and PM597 doped POF (plasmonic POF, called Au NPs doped POF) through controlling the drawn temperature of these POF preforms lower than the soft temperature of preform. Using linear polarization nano-second (ns) laser pumping, the degrees of

polarization are calculated to be 0.83, 0.94, 0.98 for the oriented long-range, short-range and plasmonic disorder POF with 1.5 cm length, respectively. In addition, the random lasing polarization property of these disorder POFs can be maintained in the different POF length. Their work provides a new way to control polarization of RL in the POF except considering add a polarizer element in the random fibre system.

2.2 Fibre grating

2.2.1 Fibre grating history

In 1978, K. O. Hill *et. al.* first reported optical fibre photosensitivity in a Ge-doped-core fibre at Communication Research Centre in Canada [70]. They used a single-mode argon-ion laser to launch into the photosensitive fibre. The standing wave pattern formed by the 4% back reflection from the fibre end interacting with the forward propagating light wave forms the periodic perturbation in the fibre, which comprises a fibre filter. Through the transmission and reflection measurement, they first demonstrated the realization of distributed feedback reflectors in the visible region light that coupled the forward- to the counter-propagating light beam. The scientific discovery of "Hill" gratings was the first demonstration of an FBG. Later, D. K. W. Lam *et. al.* used coupled mode theory [71] to build the model for the optical fibre filters. And they suggested that photosensitive phenomena in Ge-doped fibres may be caused by a two-photon process based on the dependent of inducing index change on the square of the writing power.

To obtain function FBG with arbitrary reflected wavelength limited by argon ion laser in the Hill's experiment, G. Meltz *et. al.* first reported transverse holographic method to fabricate an FBG with a desired reflected wavelength through changing the incident wavelength and the included angle between the beams by using 244 nm UV laser. This new method is a more efficient and flexible than Hill's fabricated method [72]. In 1990, G. Meltz *et. al* first reported the fabrication of TFG by using the two beams holographic method through rotating the fibre with an angle respect to the interference fringes [73]. In 1993, K. O. Hill's group, D. Z. Anderson's group, and J. R. Armitage's group independently provided phase mask method to inscribe FBG [74-76]. In 1994, K. O. Hill and co-workers fabricated in-fibre chirped Bragg gratings as dispersion compensators using a double-exposure method [77]. In

1996, A. M. Vengsarkar *et. al.* extended a new kind of LPG as low-cost, in-fibre, and band-rejection filters [78]. In 2000, P. S. Westbrook *et. al.* first demonstrated the 45°-TFG as all fibre polarizer with PER of 25 dB [79]. In 2005, K. Zhou *et.al.* obtained high PER of 33 dB 45°-TFG, and theoretically investigate 45°-TFG structures using the Green's function calculation [23]. In 2006, K. Zhou *et.al.* also first fabricated >80° TFG and researched its temperature, strain, and refractive index sensitivity [80]. The FBGs as in-fibre devices have many features in the optics area, *e.g.*, easily integration, chemical inertness, nonconductive, immunity to electromagnetic interference and the capability for multiplexing. Therefore, the FBGs have been applied in the optical communications, fibre lasers, fibre sensors etc.

2.2.2 Photosensitivity of optical fibre

Photosensitive optical fibres mean the refractive index of fibre core will permanently change under the UV irradiation effect. Since Hill first inscribed FBG in the Ge-doped fibre, the other photosensitive fibres have been reported, *e.g.*, Eu^{2+}/Al_2O_3[81], Ce^{3+}[82], phosphorus [83] and Er^{3+}/Ge[84] doped fibres. But the Ge-doped fibres have more sensitivity than other kinds of photosensitive fibres. Therefore, we will mainly present the photosensitive mechanisms for Ge-doped fibres in this section.

2.2.2.1 Photosensitivity mechanisms

There are several photosensitivity mechanisms to explain the photosensitivity in the optical fibres, such as colour-centre model [85], compaction model [86], stress-relief model [87], ionic migration model [88], permanent electric dipole model [89], electron charge migration model [90], and Soret effect [91]. Among these theories, the colour-centre model and compaction model have been regarded as the main models to explain the photosensitivity phenomenon for the Ge-doped fibres. In this section, we will present three models: colour-centre model, compaction model and stress-relief model.

(1) Colour centre model

There are three absorption bands with peak of 185, 242, 325 nm for the Ge silicate glasses [92]. The 185 nm absorption band is from GeO_2. The 242 and 325nm absorption bands are attributed to the singlet-singlet and triplet-singlet transition of GeO, respectively. In 1990, D. P. Hand and P. St. J.

Russell first proposed the colour centre model. The chemistry equation of 2.7 described the colour centres formation process [93].

$$X-Y \rightleftharpoons X^+ + Y + e^-; \; e^- + Ge(N) \rightleftharpoons Ge^-(N).$$ (2.7)
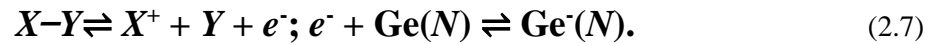
The population of oxygen-vacancy 'wrong-bonds' X—Y (Ge—Si, Si—Si and Ge—G) provides the original charge source. The absorption band of these wrong bands are around peaked in 240 and 320 nm. These bonds will be broken under the single (for example 240 nm) or multi-photon (two-photon of 480 nm) photo-ionization effect, generating GeE′ hole traps and free electrons. The free electrons will be vanished in the two ways through migrating the Ge-Si glass matrix: 1) recombining with another GeE′ site; or 2) being trapped at Ge (1) or Ge(2) dopant sites to generate Ge$^-$(1) or Ge$^-$(2) colour centres. The photo-ionization section will cause the refractive index change. The changes of refractive index induced by UV light has be calculated by Kramaers-Kronig equation as [93]:

$$\Delta n_{\text{eff}}(\lambda) = \frac{1}{2\pi^2} \rho \int_0^\infty \frac{\Delta \alpha_{\text{eff}}(\lambda)}{1-(\lambda/\lambda')^2} d\lambda.$$ (2.8)

Where, ρ is the principal part of the integral, λ' is the wavelength at which the refractive-index change, and $\Delta \alpha_{\text{eff}}(\lambda)$ is the effective change in the absorption coefficient of the defects. Although the colour centre model can explain some experimental results, it cannot make clear all experimental phenomenon [94-98], especially for the high refractive index change.

(2) Compaction and densification model

The compaction and densification model mean that materials density induced by UV laser exposure change leads to the refractive index change. In 1986, C. Fiori and R. A. B. Devine reported the linear evolution between the measured refractive index and density for the irradiated silica [86]. In the experiment, the SiO_2 sample is irradiated by 248 nm laser in the $\sim 10^{-6}$ torr at room temperature. They observed the thickness decrease by 16% at laser energy of 2000 J/cm^2. When the irradiated SiO_2 is annealed for 60 min at 950°C in vacuum of $\sim 10^{-6}$ torr, the linear compaction is reversible. But the UV irradiation energy is over the compaction threshold, the process is irreversible. From the Lorentz-Lorenz relationship for the refractivity, the refractive index differentiation can be expressed by:

$$\Delta n = -\frac{(n^2+2)(n^2-1)}{6n}(1-\frac{\Delta R}{R\Delta V/V})\frac{\Delta V}{V}. \tag{2.9}$$

Where $R = (n^2+2)/\rho(n^2-1)$, ρ is the specific gravity, n the refractive index and $\frac{\Delta V}{V}$ volume compaction. Therefore, we can calculate the refractive index based on the volume compaction. This model has been used to explain the refractive index change in other research groups' experiment [99-101].

(3) Stress relief model

The tension in the glass fibre would lead to the decrease the refractive index due to the stress-optic effect. Therefore, the stress relief will increase the refractive index of the fibre core [102]. In the Ge-doped silica fibre, the binding energy of oxygen-deficient wrong bonds (such as Ge-Si and Si-Si) is lower than that of oxygen-containing bonds [87]. The wrong bonds broken after UV laser irradiation cause the relaxation of the tensioned glass network and decrease the stress in the core of fibre. Therefore, there is different tension for the irradiation and un-irradiation section for the Ge-fibre, which lead to the different of refractive index.

2.2.3 Couple-mode theory

Coupled-mode theory has been used to analyse the propagation of electromagnetic waves in periodic layered mediums. This theory is an efficient technique to describe the fibre grating spectral characteristics. In this section, we mainly present Erdogan providing the coupled-mode theory [103-105]. In the Erdogan's work, they assumedly write the transverse component of the electric field as a superposition of the ideal waveguide modes without grating perturbation using an ideal-mode approximation to coupled-mode theory:

$$\vec{E}_t(x,y,z,t) = \sum_j [A_j(z)\exp(i\beta_j z) + B_j(z)\exp(-i\beta_j z)]$$
$$.\vec{e}_{jt}(x,y)\exp(-iwt). \tag{2.10}$$

$$\beta = \frac{2\pi}{\lambda}n_{\text{eff}}. \tag{2.11}$$

Where, j is modes order, and $A_j(z)$ and $B_j(z)$ are slowly varying amplitudes of the jth mode traveling in the $+z$ and $-z$ directions, respectively. The $\vec{e}_{jt}(x, y)$ is the transverse mode fields to describe the bound core, radiation LP modes, or cladding modes. n_{eff} is the effective refractive index for guided modes.

In the ideal waveguide, because the modes are orthogonal, the energy do not exchange. The refractive index perturbation will cause the mode couple. The evolution of amplitudes of $A_j(z)$ and $B_j(z)$ of the jth mode along z axis can be written as:

$$\frac{dA_j}{dz} = i\sum_k A_k(K_{kj}^t + K_{kj}^z)\exp[i(\beta_k - \beta_j)z]$$
$$+ i\sum_k B_k(K_{kj}^t - K_{kj}^z)\exp[-i(\beta_k + \beta_j)z]. \tag{2.12}$$

$$\frac{dB_j}{dz} = -i\sum_k A_k(K_{kj}^t - K_{kj}^z)\exp[i(\beta_k + \beta_j)z]$$
$$- i\sum_k B_k(K_{kj}^t + K_{kj}^z)\exp[-i(\beta_k - \beta_j)z]. \tag{2.13}$$

Where, K_{kj}^t and K_{kj}^z are the transverse and longitudinal coupling coefficient between modes j and k, respectively. In the equations of 2.12 and 2.13, the K_{kj}^t can be defined as:

$$K_{kj}^t(z) = \frac{\omega}{4}\iint_\infty [\Delta\varepsilon(x, y, z)\vec{e}_k^t(x, y).\vec{e}_j^{t*}(x, y)]dxdy. \tag{2.14}$$

Where, the $\Delta\varepsilon$ is the perturbation of the permittivity. When $\delta n << n$, $\Delta\varepsilon \cong 2n\delta n$. K_{kj}^z is similar with K_{kj}^t. But $K_{kj}^z << K_{kj}^t$ for the fibre modes, then the K_{kj}^z usually can be neglected.

The FBGs are fabricated by using UV laser light to expose silica fibre. The refractive index perturbation δn_{eff} can be written as:

$$\delta n_{\text{eff}} = \overline{\delta}n_{\text{eff}}(z)[1 + v\cos(\frac{2\pi}{\Lambda}z + \phi(z))]. \tag{2.15}$$

Where, $\overline{\delta}n_{\text{eff}}$ is the "dc" index change spatially averaged over a grating period, v the fringe visibility of the index change, Λ the grating period, and $\phi(z)$ the grating chirp.

In the fibre core of the most fibre grating, the refractive index change $\delta n_{\mathrm{eff}}(x, y, z)$ is approximately uniform. And for the outside of fibre core, the change can be neglected. Therefore, we can replace the $\overline{\delta} n_{\mathrm{eff}}(z)$ with $\overline{\delta} n_{\mathrm{co}}(z)$ in the equation of 2.15. Then the equation of 2.14 can be rewritten as:

$$K_{kj}^{t}(z) = \sigma_{kj}(z) + 2\kappa_{kj}(z)\cos[\frac{2\pi}{\Lambda} z + \phi(z)]. \tag{2.16}$$

Where, σ_{kj} and κ_{kj} are "dc" (period-averaged) coupling coefficient and "ac" coupling coefficient, respectively:

$$\sigma_{kj}(z) = \frac{\omega n_{\mathrm{co}}}{4} \overline{\delta} n_{\mathrm{co}}(z) \iint\limits_{\mathrm{core}} dx dy \vec{e}_{kt}(x, y).\vec{e}_{jt}^{*}(x, y). \tag{2.17}$$

$$\kappa_{jt}(z) = \frac{v}{2} \sigma_{kj}(z). \tag{2.18}$$

2.2.3.1 Fibre Bragg grating (FBG)

In a FBG, the amplitude $A(z)$ near the wavelength for which reflection of a mode coupling into an identical counter-propagating mode of amplitude $B(z)$ is the dominant interaction. The equation of 2.12 and 2.13 can be simplified as:

$$\frac{dR}{dz} = i\hat{\sigma}R(z) + i\kappa S(z); \tag{2.19}$$

$$\frac{dS}{dz} = -i\hat{\sigma}S(z) - i\kappa^{*}R(z). \tag{2.20}$$

Where the amplitudes R and S are

$$R(z) \equiv A(z)\exp(i\delta z - \phi/2); \tag{2.21}$$

$$S(z) \equiv B(z)\exp(-i\delta z + \phi/2). \tag{2.22}$$

Where κ is the "ac" coupling coefficient and $\hat{\sigma}$ is a general "dc" self-coupling coefficient defined as

$$\hat{\sigma} \equiv \delta + \sigma - \frac{1}{2}\frac{d\phi}{dz}. \tag{2.23}$$

Where detuning δ is independent of for all gratings, which is defined to be

$$\delta \equiv \beta - \frac{\pi}{\Lambda} = \beta - \beta_{D} = 2\pi n_{\mathrm{eff}}(\frac{1}{\lambda} - \frac{1}{\lambda_{D}}). \tag{2.24}$$

Where $\lambda_D \equiv 2n_{eff}\Lambda$ is the "design wavelength" for Bragg scattering by an infinitesimally weak grating ($\delta n_{eff} \rightarrow 0$) with a period Λ.

For a single-mode Bragg reflection grating,

$$\delta = 2\pi\overline{\delta}n_{eff}; \tag{2.25}$$

$$\kappa = \kappa^* = \frac{\pi}{\lambda}v\overline{\delta}n_{eff}. \tag{2.26}$$

If the FBG is uniform in the z direction, $\overline{\delta}n_{eff}$, κ, σ and $\hat{\sigma}$ are constants, and $d\phi/dz = 0$. Then the equations of 2.19 and 2.20 become coupled first-order ordinary differential equations with constant coefficients. When appropriate boundary conditions are provided, the closed-form solutions can be obtained. The reflectivity of a FBG with length of L can be obtained when assuming a forward-propagating wave incident is from $z = -\infty$ and there is not back-propagating wave exist for $z \geq L/2$. The amplitude $\rho = S(-L/2)R(-L/2)$ and power reflection coefficients $\gamma = |\rho|^2$ can be rewritten as:

$$\rho = \frac{-\kappa\sinh(\sqrt{\kappa^2 - \hat{\sigma}^2}L)}{\hat{\sigma}\sinh(\sqrt{\kappa^2 - \hat{\sigma}^2}L) + i\sqrt{\kappa^2 - \hat{\sigma}^2}\cosh(\sqrt{\kappa^2 - \hat{\sigma}^2}L)}; \tag{2.27}$$

$$\gamma = \frac{\sinh^2(\sqrt{\kappa^2 - \hat{\sigma}^2}L)}{\cosh^2(\sqrt{\kappa^2 - \hat{\sigma}^2}L) - \frac{\hat{\sigma}^2}{\kappa^2}}. \tag{2.28}$$

From the equation of 2.28, the maximum reflectivity γ_{max} for a FBG is

$$\gamma_{max} = \tanh^2(\kappa L). \tag{2.29}$$

And the γ_{max} will occurs when $\hat{\sigma} = 0$ or at wavelength

$$\lambda_{max} = (1 + \frac{\overline{\delta}n_{eff}}{n_{eff}})\lambda_D. \tag{2.30}$$

2.2.3.2 Long period grating (LPG)

In a LPG, the amplitude $A_1(z)$ near the wavelength of a mode "1" coupling into a co-propagating mode "2" of amplitude $A_2(z)$ is the dominant interaction. The equations of 2.11 and 2.12 can be simplified as:

$$\frac{dR}{dz} = i\hat{\sigma}R(z) + i\kappa S(z); \tag{2.31}$$

$$\frac{dS}{dz} = -i\hat{\sigma}S(z) + i\kappa^* R(z). \tag{2.32}$$

Where the new amplitudes R and S are

$$R(z) \equiv A_1 \exp[-i(\sigma_{11} + \sigma_{22})z/2]\exp(i\delta z - \phi/2); \tag{2.33}$$

$$S(z) \equiv A_2 \exp[-i(\sigma_{11} + \sigma_{22})z/2]\exp(-i\delta z + \phi/2). \tag{2.34}$$

Where σ_{11} and σ_{22} are "dc" coupling coefficients for the two modes, $\kappa = \kappa_{21} = \kappa_{12}^*$ the "ac" cross-coupling coefficient, and $\hat{\sigma}$ is the "dc" self-coupling coefficient that can be defined as:

$$\hat{\sigma} \equiv \delta + \frac{\sigma_{11} - \sigma_{22}}{2} - \frac{1}{2}\frac{d\phi}{dz}. \tag{2.35}$$

Where the detuning δ can be as constant along z:

$$\delta \equiv \frac{1}{2}(\beta_1 - \beta_2) - \frac{\pi}{\Lambda} = \pi\Delta n_{eff}(\frac{1}{\lambda} - \frac{1}{\lambda_D}). \tag{2.36}$$

Where $\lambda_D \equiv n_{eff}\Lambda$ is the "design wavelength" for infinitesimally weak grating.

2.2.3.3 Tilted fibre grating (TFG)

The structure of TFG is tilted by an angle θ relative to the fibre axis z', as shown in the Figure 2.13. The refractive index change δn_{co} in the core for TFG can be written as:

$$\delta n_{co}(x, z) = \bar{\delta}n_{co}(z')\{1 + v\cos[\frac{2\pi}{\Lambda_g}z' + \phi(z')]\}. \tag{2.37}$$

Where $z' = x\sin\theta + z\cos\theta$, the grating period in the fibre axis $\Lambda = \Lambda_g/\cos\theta$ that determines the coupling resonant wavelengths.

By slowly changing $\bar{\delta}n_{co}(z')$ and $\phi(z')$, when $z' = z\cos\theta$, that means we only take the projection of these functions onto the fibre axis, the coupling coefficient in the equation of 2.16 can be expressed as:

$$K_{\mp\pm}^t(z) = \sigma(z) + 2\kappa_{\mp\pm}(z)\cos[\frac{2\pi}{\Lambda}z + \phi(z\cos\theta)]. \tag{2.38}$$

Where the subscripts j and k describe the forward-propagating mode $(+)$ the other describes the backward-propagating mode for the same mode. The self and cross coupling coefficients can be expressed as:

$$\sigma(z) = \frac{\omega n_{co}}{2} \bar{\delta} n_{co}(z\cos\theta) \iint\limits_{core} dxdy \vec{e}_{\mp t}(x,y).\vec{e}_{\pm t}^*(x,y). \tag{2.39}$$

$$\kappa_{\mp\pm}(z,\theta) = \frac{v}{2}\frac{\omega n_{co}}{2} \bar{\delta} n_{co}(z\cos\theta) \iint\limits_{core} dxdy \exp(\pm i\frac{2\pi}{\Lambda} x\tan\theta)\vec{e}_{\mp t}(x,y).\vec{e}_{\pm t}^*(x,y). \tag{2.40}$$

Notice $\kappa_{\pm} = (\kappa_{\mp})^*$. The effects of tilt can be expressed by "effective fringe visibility" $v_{\mp\pm}(\theta)$, which is defined as:

$$\frac{v_{\mp\pm}(\theta)}{v} = \frac{\iint\limits_{core} dxdy \exp(\pm i\frac{2\pi}{\Lambda} x\tan\theta)\vec{e}_{\mp t}(x,y).\vec{e}_{\pm t}^*(x,y)}{\iint\limits_{core} dxdy \vec{e}_{\mp t}(x,y).\vec{e}_{\pm t}^*(x,y)}. \tag{2.41}$$

Thus, the equation of 2.40 can be rewritten as:

$$\kappa_{\mp\pm}(z,\theta) = \frac{v_{\mp\pm}(\theta)}{2}\sigma(z). \tag{2.42}$$
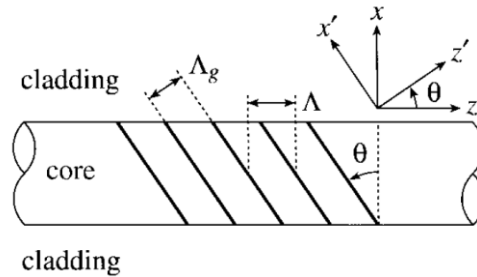
Figure 2.13 Diagram of a TFG in the fibre core [103].

2.3 Chapter conclusion

In this first part of the chapter, we give a review on RLs and RFLs development history. And then the ways realizing polarized random lasing and random fibre lasing emission has been given, including anisotropic absorption, scattering, adding polarized elements, or graphene. In the second part of this chapter, we review the grating development history and the UV-induced photosensitivity mechanisms, *e.g.*, colour centre, compaction/densification and stress relief. Finally, the mode coupling theory for the FBG, LPG and TFG have been discussed in detail.

Chapter 3. Spectral Characteristics of Fibre Grating and Sensing Applications

3.1 Introduction

In this chapter, the spectral characteristics of TFG, FBG and LPG will be theoretical analysed. Furthermore, the measurements of spectral characteristics for TFG, FBG and LPG will be researched. This will be followed by a detailed research for the temperature sensing of TFG with small angle and LPG. Finally, the stress sensing application of FBG will be discussed.

3.2 Phase-Match conditions for fibre grating

When the light propagates in the fibre grating [106], the strongest light coupling will take place for satisfying the phase-match condition.

$$\boldsymbol{K}_{\text{out}} = \boldsymbol{K}_{\text{in}} + \boldsymbol{K}_{\text{G}} \,. \tag{3.1}$$

Where $\boldsymbol{K}_{\text{out}}$, $\boldsymbol{K}_{\text{in}}$, and $\boldsymbol{K}_{\text{G}}$ are wave vectors for radiated light, incident mode, and fibre grating itself, respectively. And $\boldsymbol{K}_{\text{in}} = \dfrac{2\pi}{\lambda}.n_{\text{co}}$ and $\boldsymbol{K}_{\text{G}} = \dfrac{2\pi}{\Lambda_{\text{G}}}$. Where n_{co} is the effective index of fire core, Λ_{G} is the normal period of fibre grating. Figure 3.1 and 3.2 show the phase matching condition for a fibre grating, which can be described in a vectorial plane. Figure 3.1(a) shows the mode coupling of a FBG. When the light propagates in the FBG, the core mode in the forward-propagating will be coupled into backward propagating core mode due to $\boldsymbol{K}_{\text{out}} = \boldsymbol{K}_{\text{in}} = \dfrac{2\pi}{\lambda}.n_{\text{co}}$. When the light propagates in the LPG, the core mode in the forward-propagating will be coupled into forward-propagating cladding modes with $\boldsymbol{K}_{\text{out}} = \boldsymbol{K}_{\text{in}} = \dfrac{2\pi}{\lambda}.n_{\text{cl,m}}$. Where $n_{\text{cl,m}}$ is effective index of fibre core.

A TFG can couple out light from fibre core in the diverse directions. The strongest coupled light wavelength can be determined by the phase-match condition as:

$$\lambda_{\text{co-cl}} = (n_{\text{co}} \pm n_{\text{cl,m}}).\dfrac{\Lambda_{\text{G}}}{\cos\theta}\,; \tag{3.2}$$

Where $n_{\text{cl,m}}$ is effective index of fire core for the mth cladding mode, The "+" ("-") indicates the mode propagates in the $-z$ ($+z$) direction. As shown in the Figure 2.13, Λ is the period along fibre axis.

The TFGs can be classified into three regimes depending on the tilt angle θ: 1) When $\theta = 45^{\circ}$, as shown in the Figure 3.2 (a), the core mode in the forward-propagating will be coupled into radiation

mode and propagated out from the fibre side; 2) When the $\theta > 45^\circ$ (Figure 3.2 b) or $\theta < 45^\circ$ (Figure 3.2 c) , the core mode will be coupled into forward-propagating and back-propagating radiation and cladding modes, respectively. Because the refractive index of fibre core and cladding is close, the difference of $\boldsymbol{K}_{in}$ and $\boldsymbol{K}_{out}$ can be neglected.
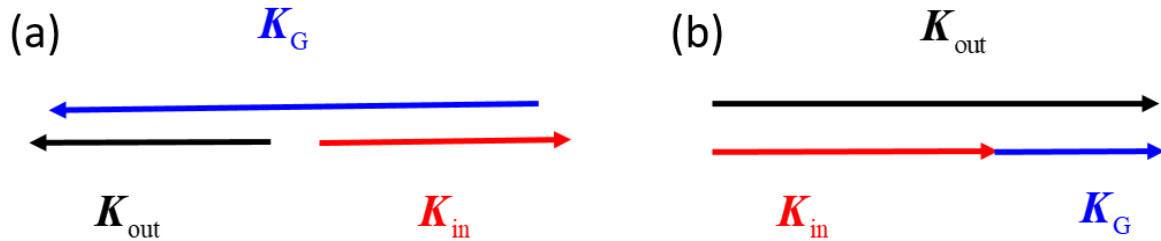
Figure 3. 1 The wave vectors relationship of $\boldsymbol{K}_{out}$, $\boldsymbol{K}_{in}$, and $\boldsymbol{K}_G$ for FBG (a) and LPG (b).
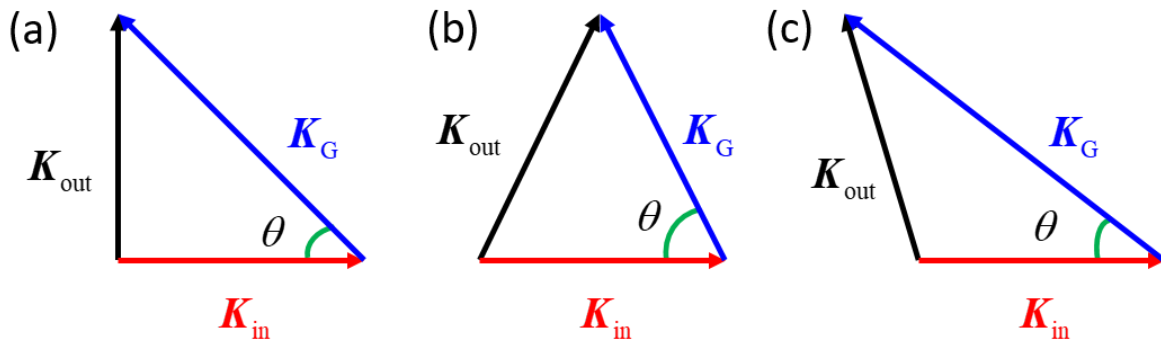
Figure 3. 2 The wave vectors relationship of $\boldsymbol{K}_{out}$, $\boldsymbol{K}_{in}$, and $\boldsymbol{K}_G$ for TFGs with different tilted angles: $\theta = 45^\circ$ (a), $\theta > 45^\circ$ (b), $\theta < 45^\circ$ (c).

3.3 Spectral characteristics of fibre grating

3.3.1 Transmission of fibre grating

Figure 3.3 shows the experiment setup to measure the transmission of fibre gratings (FG). The broadband light source (BBS, 1550A-TS, AFCor83437A, Agilent) is as signal light, which propagates into fibre grating including small angle TFGs, 45º TFG, FBG, and LPG. The transmission will be collected by optical spectrum analyzer (OSA, Hewlett Packard, 86142A).

These fibre gratings have been fabricated using a 244nm UV laser and phase-mask scanning method in the hydrogen-loaded standard SMF. To research the effect of the tilted angles on the radiation mode out-coupling of TFGs, we measure the transmission spectra of small angle with 1º, 3º, 7º, and 45º TFG. We use "BBS 1550A-TS, AFC" broadband light source as signal light with band wide of 1500-1600

nm. Figure 3.4 shows the transmission spectra of TFGs with different tilted angles. It can be seen that when the tilted angle increases the number of the radiation out-coupling mode increases. There are more light have been coupled into backward-propagating cladding modes (not the backward-propagating core modes) by the TFG for large tilted angle. When the tilted angle increase at 3º and 7º, we observe the comb-like resonances for the cladding mode couplings. In addition, the central wavelength of the comb-like resonances occurs blue-shift effect with the tilted angle increasing from the transmission-loss profile. And the range of the comb-like resonances increases. When these TFGs have been immersed in index-matching gel, the comb-like resonances disappeared. We can use the comb-like resonances wavelength as the sensitive wavelength. Meanwhile, there are Bragg resonance existing in the small angle TFG in the longer wavelength side of the radiation profile. When the tilted angle is 1º, 3º, 7º, corresponding the Bragg resonance wavelength peaks located in 1551.1 nm, 1553.7 nm, 1581.9 nm. The Bragg resonance wavelength occurs red-shift with the increase of tilted angle.
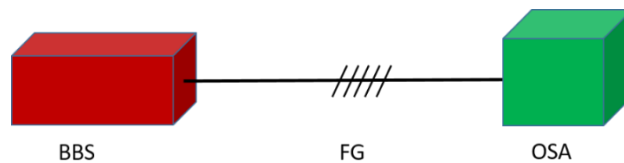
Figure 3. 3 The experimental setup to measure transmission for fibre grating (FG).
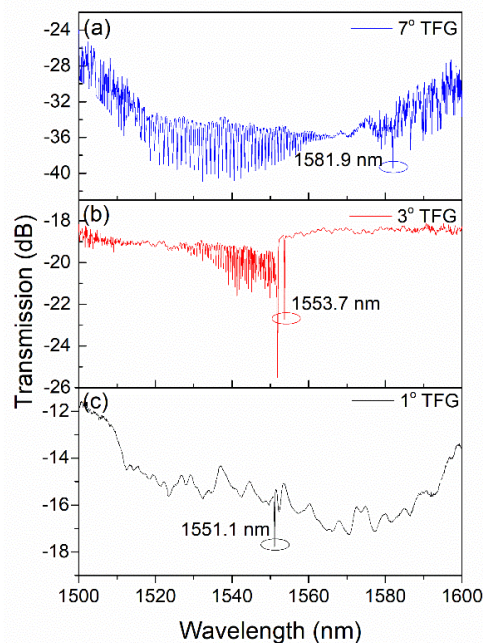
Figure 3. 4 The transmission of TFG with different tilted angles: (a) 7º; (b) 3º; (c) 1º.

Figure 3.5 shows the transmission-loss profile of 45° TFGs. The experimental setup is the same for the small angles TFG. The transmission of 45°TFGs is not like that of small angles TFG. The comb-like resonances wavelengths disappear. The ripple characteristics in the transmission is attributed to the unmatched refractive index at the boundary between the cladding and air.
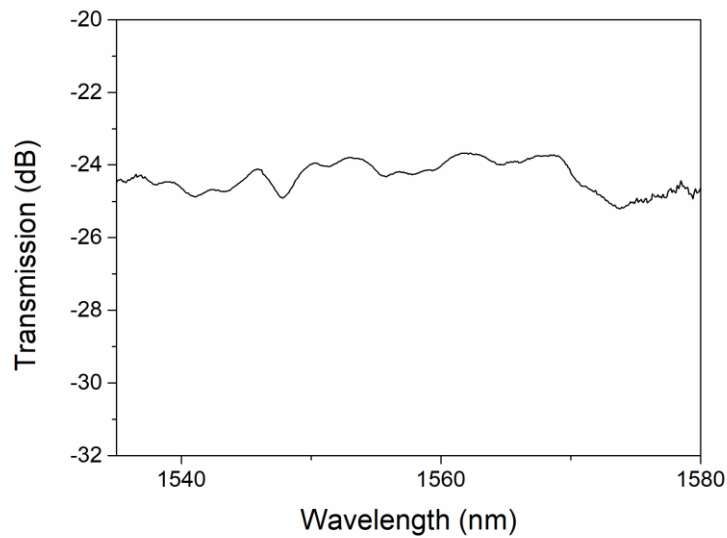
Figure 3. 5 The transmission of 45° TFG.

Figure 3.6 shows the transmission-loss profile of FBG. The experimental setup is the same for the small angles and 45° TFG. This is the typical transmission spectra of FBG. The dip located in the 1551.6 nm. The forward-propagating mode at this wavelength has been reflected to back-propagating core mode by FBG.
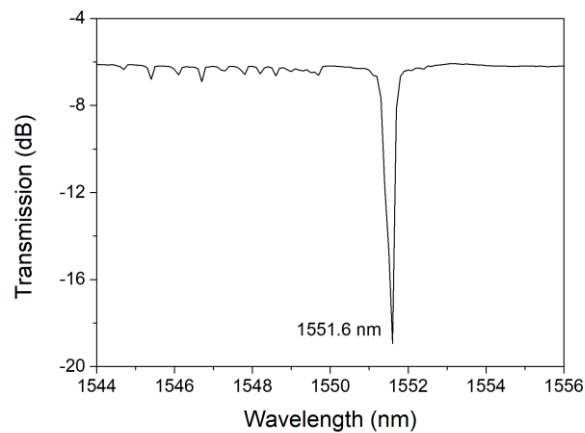
Figure 3. 6 The transmission spectrum of FBG.

Figure 3.7 shows the transmission-loss profile of LPG with period of 480μm. The experimental setup is the same for the small angles and 45°TFG.But the light source has been changed as "83437A, Agilent". It can be seen that there are 11main distinct resonant loss band in the wavelength range of from 1200-1600 nm, which is caused by the coupling of the fundamental core mode (LP_{01}) to the forward-propagating cladding modes [107]. At room temperature, the loss peaks locate in 1283.2 nm, 1386.8 nm, 1409.2 nm, 1420.8 nm, 1447.2 nm, 1466.4 nm, 1494.4 nm, 1532.8 nm, 1548.8nm, 1562.4nm, 1592.4 nm, corresponding to be marked as P01, P02, P03, P04, P05, P06, P07, P08, P09, P10, P11. The coupled cladding mode dips have reached at -7.390 dB, -3.099 dB, -5.110 dB, -5.351 dB, -6.144 dB, -5.694 dB, -10.594 dB, -5.267 dB, -4.009 dB, -5.074 dB, -2.768 dB for P01-P11, respectively. The LPG has coupled the light from the fundamental core mode to co-propagating cladding modes in the fibre, which can be applied in the fibre sensors.
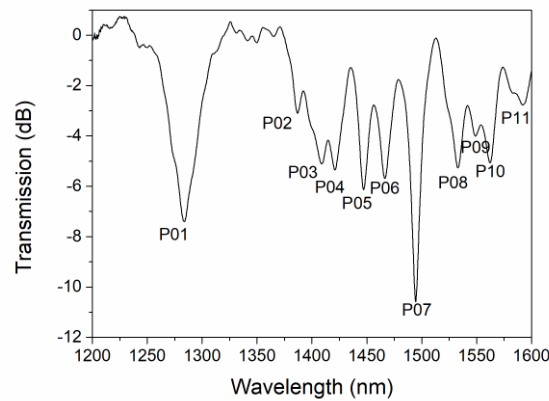
Figure 3. 7 The transmission spectrum of LPG.

3.3.2 PER of TFG

When the unpolarised light incidences on the boundary between two media with different refractive indices, the reflected light and refracted light become partially polarized light. When the incidence angle reaches to the Brewster angle, the reflected light become totally polarized light and refracted light becomes partially polarized light [108]. Based on the Snell's law, the Brewster angle can be obtained as:

$$\theta_B = \arctan(\frac{n_2}{n_1}).$$ (3.3)

Where n_1 and n_2 is the refractive index of the two media, respectively. In the TFG, the value of n_1 is equal to the effective refractive index of fibre core, and n_2 is the effective refractive index for the UV-irradiated fibre core. The refractive index change after UV-irradiated is very small, which is about the order of $10^{-5} \sim 10^{-3}$. Thus, $n_2 = n_1$. Therefore, the Brewster angle can be calculated as $\theta_B = \arctan(n_1/n_2) = \arctan(1) = 45^\circ$ in the TFG. It can be seen that the 45° TFG can be as an ideal in-fibre polarizer. When the un-polarized light propagates in the 45° TFG, the *s*-polarized light will be coupled out from fibre core and *p*-polarized light will propagate through the fibre core, which is shown in the Figure 3.8. K. Zhou *et. al.* obtained a high polarization-extinction ratio of 33 dB near 1550 nm in the 45° TFG. And they theoretically research the relationship between the polarization property and the tilted angles of TFG based on the Green's function calculation [23]. In this section, we will research the PER property of small angle and 45° TFG.
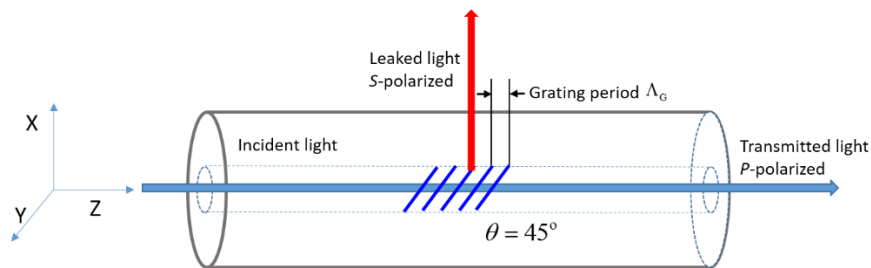
Figure 3. 8 The Schematic of polarization function of a 45°-TFG.

The PER represents the peak-to-peak difference in the transmission of optical component or system for the all the possible polarization states [109]. Figure 3.9 shows the experimental setup to measure PER by the polarization scanning technique. The light from BBS propagates through fibre polarizer (P) and becomes polarized light. And the polarization of the polarized light will be controlled by polarization controller (PC). Finally, the polarized light propagates TFG and is collected by OSA.
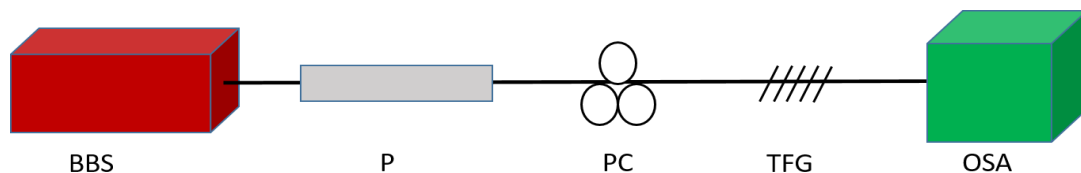
Figure 3. 9 The PER measurement schematic of the TFG.

Figure 3.10 shows the maximum and minimum transmission for small angle TFG with 1º, 3º and 7º. There is no or few polarization effects for 1º and 3º TFG, as shown in Figure 3.9 (a) and (b). Figure 3.9(c) shows the two orthogonal polarization states. It can be seen that the comb-like resonances are polarization dependent. The maximum PER value for 7º TFG is 4.5 dB. Figure 3.11shows that magnified comb-like resonances transmission for two orthogonal polarization states. We can see that there are two sets of polarization dependent peaks. When the light is P_{min} polarization state, the sets of resonances spectrum for P_{max} disappear and vice versa. And the cladding mode shift for the orthogonal polarization states is 0.05 nm. And the FWHM is 0.45 nm.
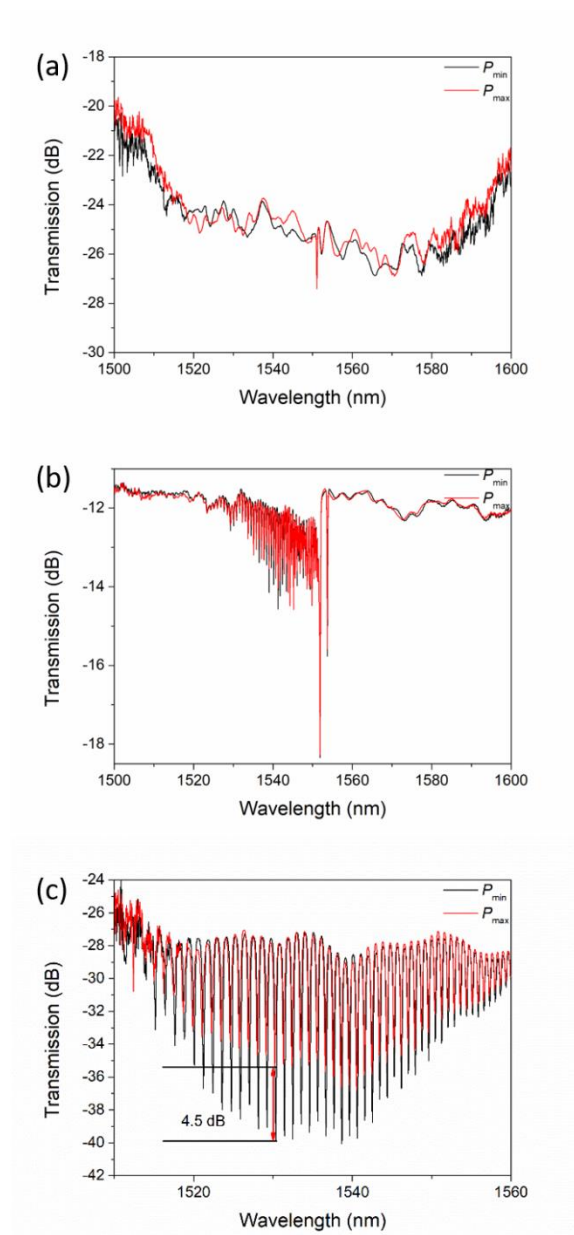
Figure 3. 10 The maximum and minimum transmission for the small angle TFG with 1º (a), 3º (b), 7º (c).
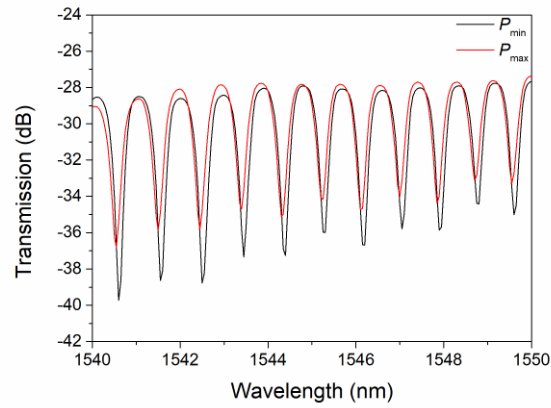
Figure 3. 11 The magnified maximum and minimum transmission for the small 7º TFG.

Figure 3.12 shows the maximum and minimum transmission for 45º TFG with grating length 24mm. The transmission for the 45ºTFG is polarization dependent. The maximum PER is 14 dB, which is lower than Zhou's reported 45º TFG with >30 dB [23]. The reason is that the grating length of 45º TFG in our work is lower than that in the Zhou's work. But the polarized property of 45º TFG is better than small angle TFG.
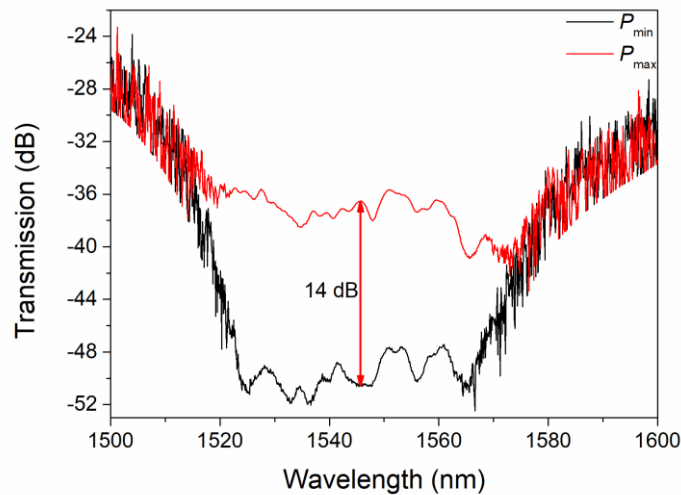
Figure 3. 12 The maximum and minimum transmission for the 45º TFG.

3.4 Applications of fibre grating

3.4.1 Temperature sensing application of fibre grating

The environment temperature and strain will affect the effective refractive index and grating period of fibre grating. Therefore, the fibre grating can be as temperature sensors and stress sensors based on the central wavelength shift.

47

For the FBG, the effect of temperature and strain changes on the wavelength shift are given as:

$$\Delta\lambda_B = 2(\Lambda \frac{\partial n_{\text{eff}}}{\partial T} + n_{\text{eff}} \frac{\partial \Lambda}{\partial T})\Delta T + 2(\Lambda \frac{\partial n_{\text{eff}}}{\partial l} + n_{\text{eff}} \frac{\partial \Lambda}{\partial l})\Delta l \ . \tag{3.4}$$

The first term in the equation of 3.4 is the thermal effect for the FBG. The thermal effect will result in two changes: 1) thermal expansion increasing grating period; 2) temperature increase inducing the increase of effective refractive index. The first term can be defined as:

$$\Delta\lambda_B = \lambda_B (\alpha_\Lambda + \alpha_n)\Delta T \ ; \tag{3.5}$$

$$\alpha_\Lambda = \frac{1}{\Lambda}\frac{\partial \Lambda}{\partial T}; \quad \alpha_n = \frac{1}{n_{\text{eff}}}\frac{\partial n_{\text{eff}}}{\partial T} \ . \tag{3.6}$$

Where α_Λ is the fibre thermal expansion coefficient, and α_n is the thermos-optical coefficient.

For the LPG, there is distinct resonant loss bands in the transmission spectra due to the coupling of the fundamental core mode (LP$_{01}$) to the forward-propagating cladding modes (LP$_{0m}$).Based on the phase-matching condition [78, 107], the resonance wavelength λ_{res} of the LPG with grating period Λ is determined as:

$$\lambda_{\text{res}} = (n_{\text{co}}^{\text{eff}} - n_{\text{cl,m}}^{\text{eff}})\Lambda. \tag{3.7}$$

Where $n_{\text{co}}^{\text{eff}}$ and $n_{\text{cl,m}}^{\text{eff}}$ are the effective indexes for the fundamental fibre core mode and m_{th} cladding mode, respectively. The equation of 3.7 can be derived for the temperature sensitivity $d\lambda_{\text{res}}/dT$ as:

$$\frac{d\lambda_{\text{res}}}{dT} = \lambda_{\text{res}} \cdot \gamma \cdot (\alpha + \Gamma_{\text{temp}}) \ ; \tag{3.8}$$

Where α is the thermal expansion coefficient for the LPG. γ is the waveguide dispersion, which can be written as [110, 111]:

$$\gamma = \frac{\dfrac{d\lambda_{\text{res}}}{d\Lambda}}{n_{\text{co}}^{\text{eff}} - n_{\text{cl,m}}^{\text{eff}}} \ . \tag{3.9}$$

Γ_{temp} is temperature dependence of the waveguide dispersion, which can be described as:

$$\Gamma_{\text{temp}} = \frac{\xi_{\text{co}} n_{\text{co}}^{\text{eff}} - \xi_{\text{cl}} n_{\text{cl,m}}^{\text{eff}}}{n_{\text{co}}^{\text{eff}} - n_{\text{cl,m}}^{\text{eff}}} \ . \tag{3.10}$$

Where ξ_{co} and ξ_{cl} are the thermal-optical coefficients, respectively.

For the TFG, based on the phase-matching condition in the equation 3.2 the Bragg reflected wavelength λ_B and cladding resonance wavelength $\lambda_{cl,m}$ can be expressed as:

$$\lambda_B = 2n_{eff}\Lambda / \cos\theta\,; \tag{3.11}$$

$$\lambda_{cl,m} = (n_{co,m}^{eff} + n_{cl,m}^{eff})\Lambda / \cos\theta\,. \tag{3.12}$$

Where n_{eff}, $n_{co,m}^{eff}$ and $n_{cl,m}^{eff}$ are the effective indexes of the core mode at λ_B, core mode and m_{th} cladding mode at $\lambda_{cl,m}$, respectively. The effect of temperature and strain changes ($\Delta\varepsilon$) on the Bragg and cladding mode wavelength shifts ($\Delta\lambda_B, \Delta\lambda_{cl,m}$) are given as:

$$\Delta\lambda_B = 2(\frac{\Lambda}{\cos\theta}\frac{\partial n_{eff}}{\partial T} + \frac{n_{eff}}{\cos\theta}\frac{\partial\Lambda}{\partial T})\Delta T + 2(\frac{\Lambda}{\cos\theta}\frac{\partial n_{eff}}{\partial\varepsilon} + \frac{n_{eff}}{\cos\theta}\frac{\partial\Lambda}{\partial\varepsilon})\Delta\varepsilon\,; \tag{3.13}$$

$$\Delta\lambda_{cl,m} = (\frac{\Lambda}{\cos\theta}\frac{\partial(n_{co,m}^{eff} + n_{cl,m}^{eff})}{\partial T} + \frac{n_{co,m}^{eff} + n_{cl,m}^{eff}}{\cos\theta}\frac{\partial\Lambda}{\partial T})\Delta T$$
$$+ 2(\frac{\Lambda}{\cos\theta}\frac{\partial(n_{co,m}^{eff} + n_{cl,m}^{eff})}{\partial\varepsilon} + \frac{n_{co,m}^{eff} + n_{cl,m}^{eff}}{\cos\theta}\frac{\partial\Lambda}{\partial\varepsilon})\Delta\varepsilon \tag{3.14}$$

Figure 3.13 shows the setup of fibre gratings temperature sensing experiment. The fibre gratings are put on a thermal Peltier connected with a temperature controller (ILX Lightwave, LDT-5910B) to change the temperature from 0 ºC to 80 ºC at a step of 10 ºC. The fibre gratings are fixed on the metal heated plate (HP) on the Peltier by using thermal stable tape to avoid the influences of strain and bending.
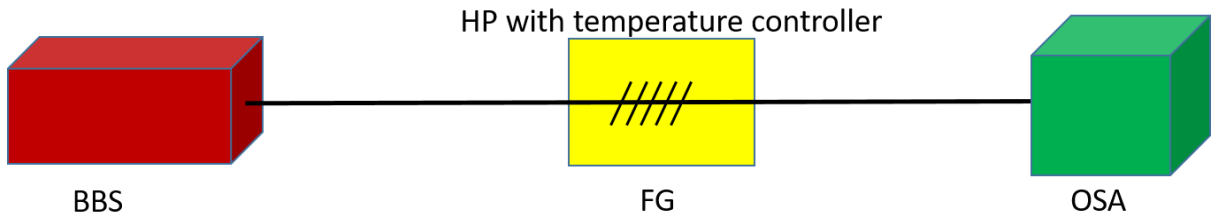
Figure 3. 13 The temperature sensing measurement schematic of the fibre gratings.

Figure 3.14 shows the transmission spectra of FBG at different temperatures. When the temperature increases from 0 ºC to 80 ºC, the dip occurs red-shift from 1551.299 to 1552.283 nm. The red-shift effect for the FBG is attributed to silica material with positive thermal-optical coefficient. From the

relationship between the temperature and dip wavelength shown in the Figure 3.15, the temperature sensitivity is 12.00±0.097 pm/°C.
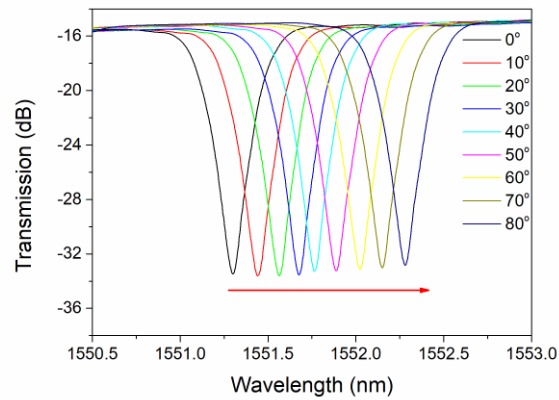
Figure 3. 14 The transmission spectra of FBG at different temperature.
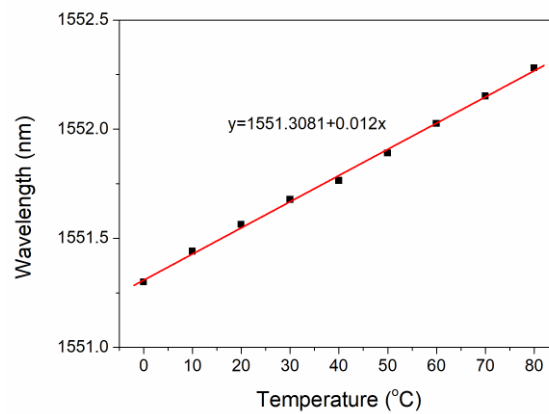
Figure 3. 15 The relationship between the temperature and dip wavelength for the FBG.

Figure 3.16 shows the transmission spectra of LPG with grating period of 480 μm at different temperatures. When the temperature increases from 0 °C to 80 °C at a step of 10 °C, all dips occur red-shift. We select 4 main dips to research the thermal sensitivity. Figure 3.17 shows the magnified transmission spectra for the dip P01, P02, P03, and P04. When the temperature increases, all the dips shift to longer wavelength. From Figure 3.18, the thermal sensitivity of P01, P02, P03, and P04 are 59.3 pm/°C, 297.1 pm/°C, 97.7 pm/°C, and 203.4pm/°C in the temperature range of 0-80 °C, respectively. The P02 dip has highest temperature sensitivity.
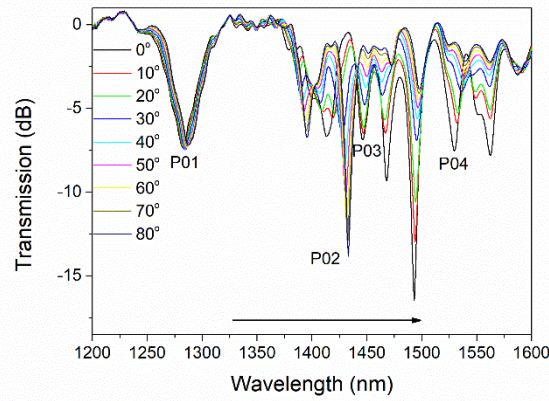
Figure 3. 16 The transmission spectra of LPG at different temperature.
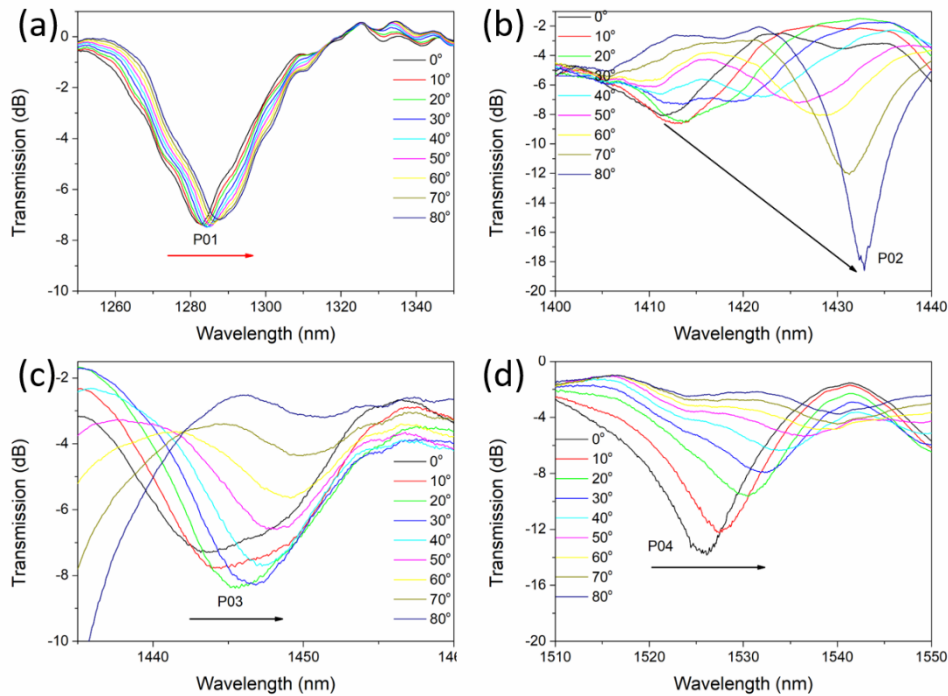
Figure 3. 17 The magnified transmission spectra of LPG at different temperature in the P01 (a), P02 (b), P03 (c), P04 (d).

Figure 3.19 shows the transmission spectra of 7° TFG at different temperature. The comb-like resonance dips wholly red-shift with temperature increasing. We choose 6 resonance dips to research the thermal sensitivity in the range of 1520-1560 nm. From the relationship between the wavelength and temperature, as shown in the Figure 3.20, the thermal sensitivity of the 7° TFG at 1520.80 nm, 1528.84 nm, 1534.24 nm, 1540.28 nm, 1546.72 nm, 1554.88 nm are 10.7 pm/°C, 11.5 pm/°C, 11.1 pm/°C, 11.3 pm/°C, 11.3 pm/°C, 11.7 pm/°C in the range of 0-80 °C, respectively. The thermal sensitivity of 7° TFG

is almost same with that of FBG (12 pm/^{o}C), however, which is much less than that of LPG with highest

thermal sensitivity of 297.1 pm/^{o}C.
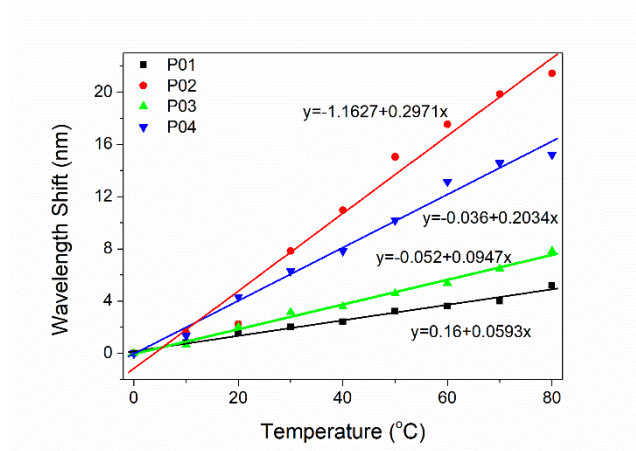
Figure 3. 18 The relationship between wavelength shift and temperature for the LPG.
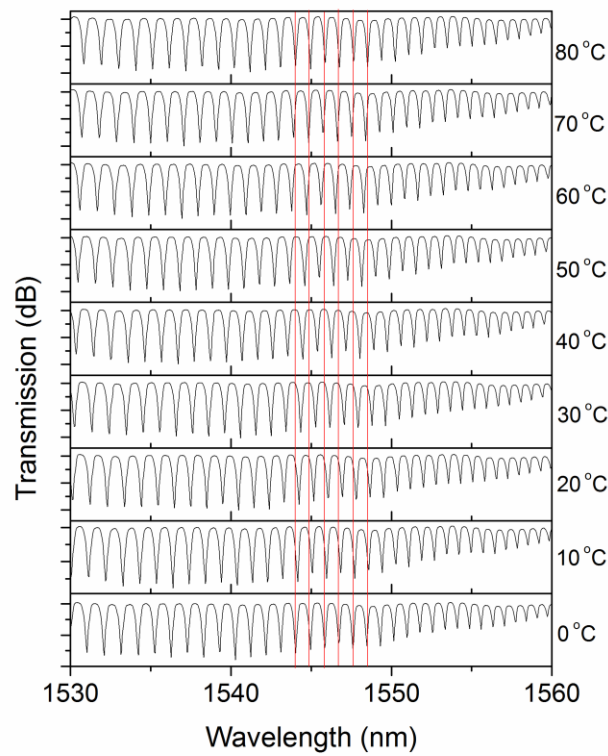
Figure 3. 19 The transmission spectra of 7° TFG at different temperature.

Figure 3. 20 The relationship between wavelength shift and temperature for 7° TFG.

3.4.2 Stress sensing application of fibre grating of FBG

In the Equation 3.4, the second term is the effect of the strain effect on the FBG. The strain will result in the change of the refractive index and grating period of the FBG. The wavelength shift can be presented as:

$$\Delta\lambda_B = \lambda_B(1 - p_e)\varepsilon_z; \tag{3.15}$$

$$p_e = \frac{n_{\text{eff}}^2}{2}[p_{12} - \nu(p_{11} + p_{12})]. \tag{3.16}$$

Where p_e is the effective strain-optic coefficient, p_{11} and p_{12} are the components of strain-optical tensor, ν is the Poisson's ratio.

Figure 3.21 shows the experimental setup for FBG strain sensitivity. The FBG was straightly placed on a group of 3D translation stage (TS) with space L of 203.5 mm. The left-hand TS has been fixed. Through removing the right-hand stage, the varied strain can be loaded to FBG from 0 mm to 0.6 mm at a step of 0.1 mm. The maximum strain is 2948 μɛ. Figure 3.22 shows the transmission spectra of the FBG with the different displacement. With the increase of the displacement, the transmission loss dip removes to long-wavelength. From the relationship between the dip wavelength and the strain, as shown in the Figure 3.23, the strain sensitivity is 0.71±0.01 pm/μɛ.
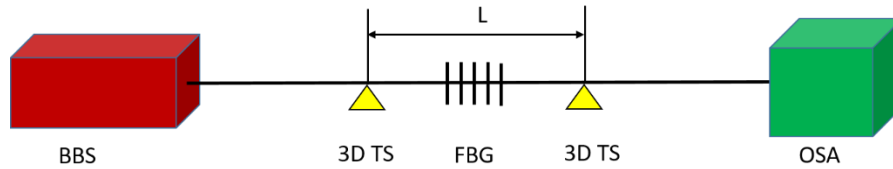
Figure 3. 21 The experimental setup for the FBG strain sensitivity measurement.
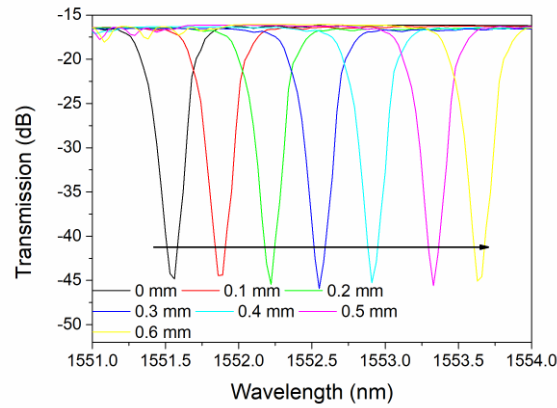
Figure 3. 22 The transmission spectra of FBG with different strain.
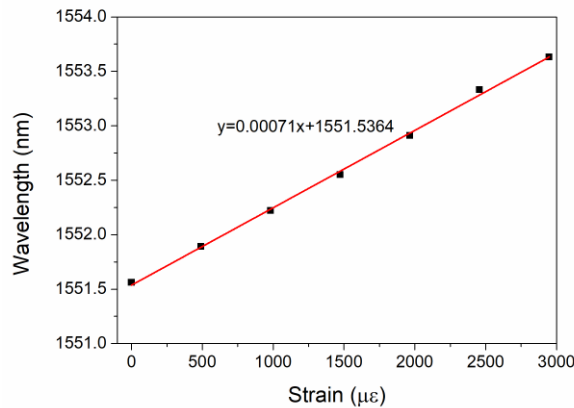
Figure 3. 23 The transmission spectra of FBG with different strain.

3.5 Chapter conclusions

In this chapter, I first have investigated phase-match conditions, transmission spectra, PER for different types of fibre grating including the TFG, FBG and LPG. We find 45° TFG has high PER with 14 dB. The 7° TFG has comb-like resonance transmission. And then we present the experimental research of the thermal sensing of different types of fibre grating. LPG with grating period of 480 μm has highest thermal sensitivity with 297.1 pm/°C among FBG, small angle TFG, LPG. Finally, we research the strain sensing of FBG. The sensitivity of the FBG is 0.71±0.01 pm/°C.

Chapter 4. Polarized Random Fibre Laser

Based on the 45º TFG

4.1 Introduction

Polarization is very important in the RFL. In the polarized RFL system, the photonic-photonic conversion efficiency is enhanced. In addition, the polarized random lasing is high quality light, which can be applied in the sensors and communications. In this chapter, I first research the random lasing emission in the SMF based Raman gain and Rayleigh scattering. The local birefringence along SMF is strongly disturbed by external perturbations, which leads to the deterioration of the polarization of RLs characteristics. Therefore, to obtain polarized RFL it should add polarization elements or induce anisotropic structure, *e.g.*, long PM optical fibre, in the fibre system, which lead to the polarized RFL system become complicated. In the Chapter 3, we know the 45º TFG has high PER. Meanwhile, 45º TFG has unique features, such as low cost, in-line fibre, easily integration. Therefore, we will use the feature of 45º TFG to obtain polarized RFLs.

4.2 Raman distributed feedback system

Figure 4.1 shows the experimental setup to research the random fibre lasing. The Raman fibre laser (1455 nm, IPG) is used to pump the SMF with length of 20.1 km through a 1455/1550-1600 nm wavelength division multiplexer (WDM). The back-scattered random lasing from SMF will be collected by an OSA (Hewlett Packard, 86142A). The SMF provides Raman gain and distributed Rayleigh scattering, which will boost the random fibre lasing emission. To avoid the Fresnel reflection of the fibre ends, all fibre ends have been spliced with APC fibre.
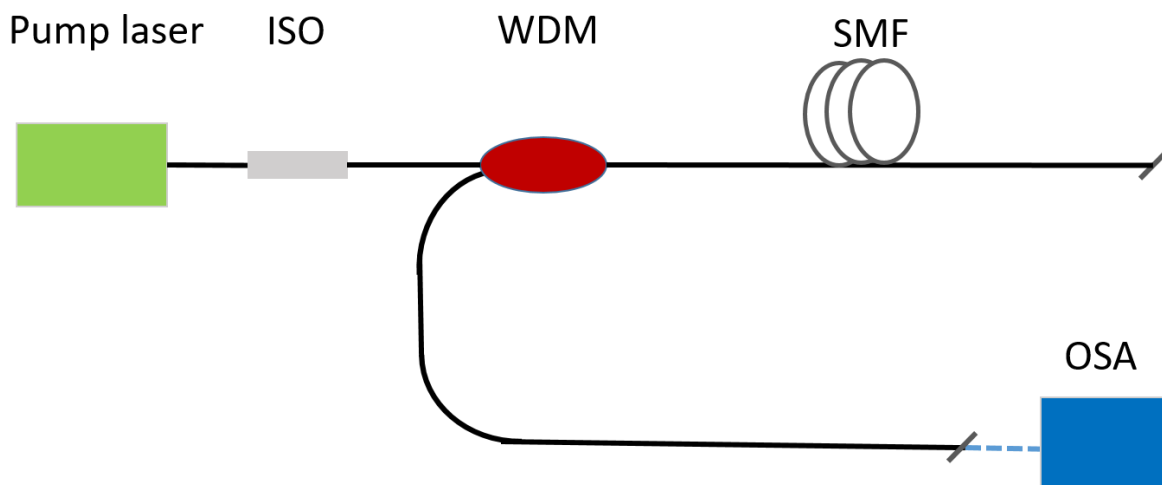
Figure 4. 1 The experimental setup to research RFLs in the Raman distributed feedback system.

4.2.1 Raman gain

Figure 4.2 shows the Raman gain spectra at different pump power. At the low pump power, there are three Raman gain peaks locating in the 1555.6 nm, 1566.0 nm and 1594.7 nm in the range of 1500-1600 nm, which accord with the Raman gain profile of silica optical fibres [112]. The maximum Raman gain shift for silica fibre is 13.2 THz. When the pump laser is 1455 nm, the maximum Raman gain wavelength is calculated to be 1554.5 nm. The small error is caused by the different between of experimental temperature and theoretical calculated temperature or the experimental error. From the relationship between the Raman gain emission intensity and pump power at 1555.6 nm, 1566.0 nm and 1594.7 nm, as shown in the Figure 4.3, we can see the Raman gain increases with the increase of pump power for the three gain peaks.
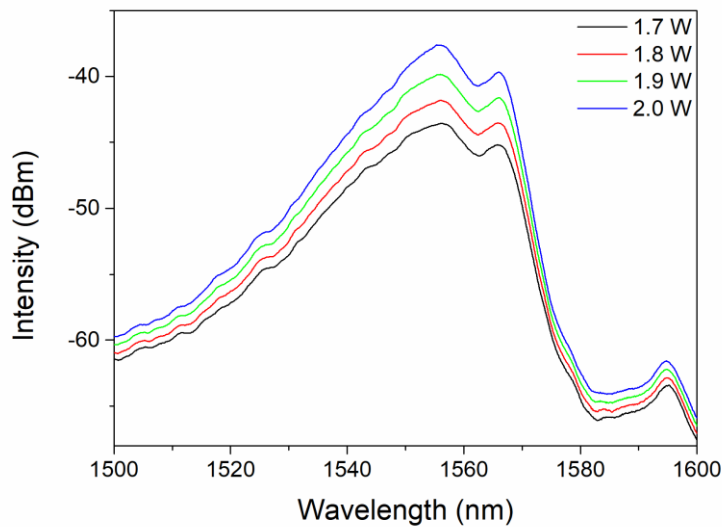
Figure 4. 2 The Raman gain spectra at different pump power.
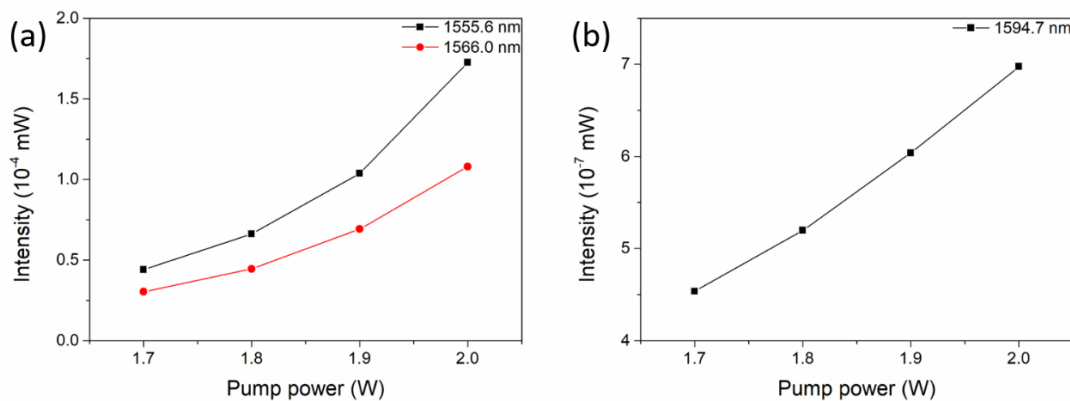
Figure 4. 3 The relationship between the Raman gain emission intensity and pump power at 1555.6 nm and 1566.0 nm(a); and 1594.7 nm (b).

4.2.2 Random lasing

With the increase of pump power, there occurs random lasing emission in the SMF system. Figure 4.4 shows the random fibre lasing emission spectra at different pump power. When the pump power increases at 2.1 W, it can be seen that the random lasing start emergence. The distributed Rayleigh backscattering provides a sufficient feedback to boost the random lasing emission [18, 113-114]. However, during the experimental measurement the random fibre lasing wavelength cannot be stabilized in range of pump power of 2.10 W and 2.66 W. These random lasing spectra are near the lasing threshold and locate in the non-stationary regime. Meanwhile, the random lasing emerges near the maximum Raman gain. In the non-stationary regime, the modes number increases with the increase of pump power from 2.10 W to 2.50 W. When the pump power increases from 2.60 W to 2.66 W, the modes number become less and the random lasing wavelength gradually start to stabilize.
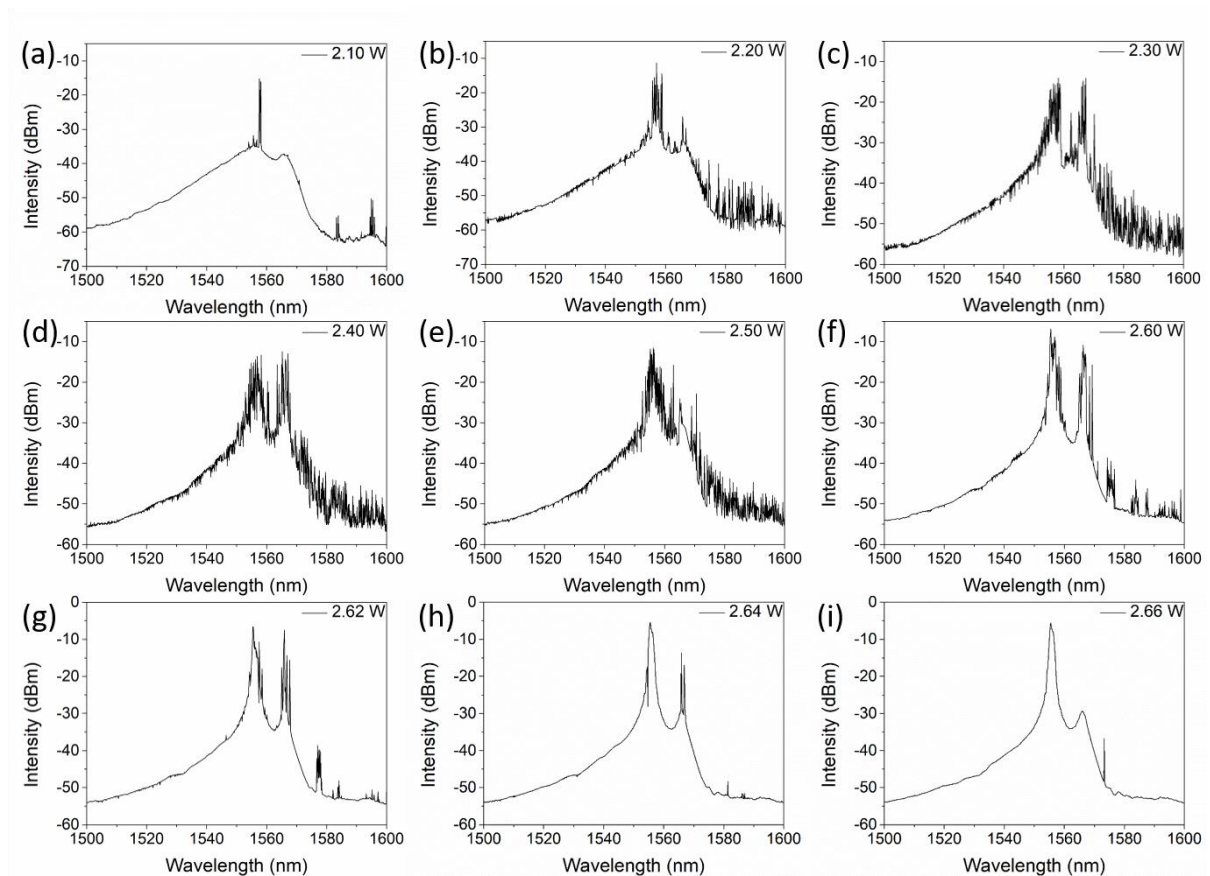
Figure 4. 4 The random lasing spectra in the non-stationary regime with different pump power from 2.10 W to 2.66 W (a-f).

When the pump power future increases, the random fibre lasing turns into stationary regime. Figure 4.5 shows the random lasing spectra in the stationary regime with different pump power from 2.68 W to

3.00 W. It can be seen that the random lasing wavelength peaks locates in the 1555.6 nm and 1566.0nm, which matches with the Raman gain spectra peaks. Figure 4.6 shows the random lasing spectra at pump power of 2.68 W using mW units. There is a shoulder peak of 1556.2 nm in the near of 1555.6 nm. We use Gauss profile to separate the two peaks and obtain the FWHM of 1555.6 nm with 0.8 nm. The narrow effect is the typical features of random lasing.
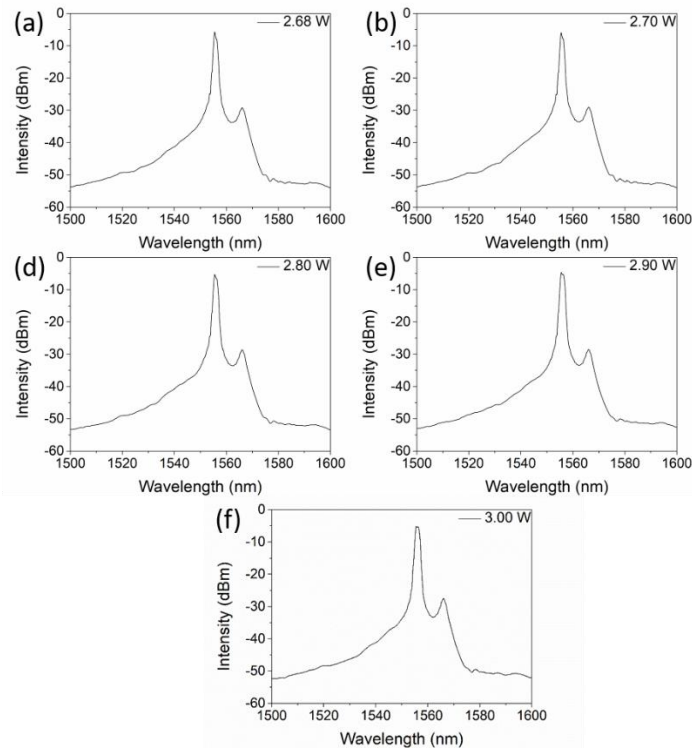
Figure 4. 5 The random lasing spectra in the stationary regime with different pump power from 2.68 W to 3.00 W (a-f).
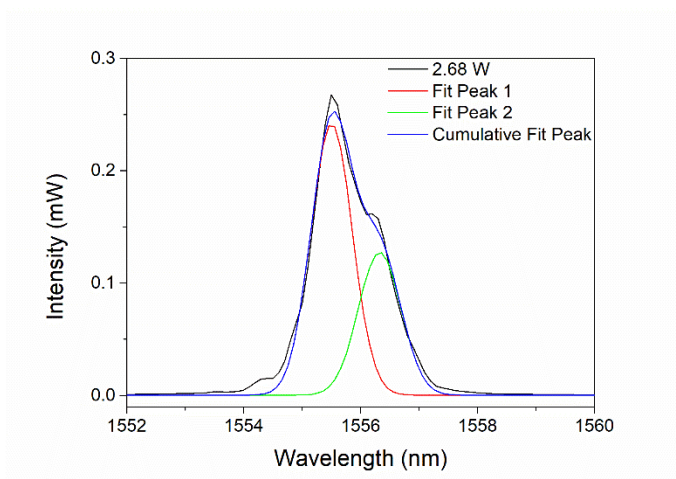
Figure 4. 6 The random lasing spectrum at pump power of 2.68 W.

From Figure 4.2, 4.4, 4.5, we can see the different experimental phenomenon. In the low pump power, the gain is larger than the lasing loss. Therefore, there is only Raman gain. When the pump power

increases, the gain is larger than the loss. But there are many mode competitions in the RFL system. The random lasing can be fixed. When the pump power increases sequentially, there are two predominant random lasing modes at 1556.2 nm and 1555.6 nm. Therefore, the random lasing wavelength can be fixed.

Figure 4.7 shows the main peak random fibre lasing stability at different pump power. The random lasing main peak wavelength almost keep constant. There is only 0.1 nm shift, which would be caused by the OSA resolution (0.1 nm) error. In the stationary regime, the random lasing mode competition tend to be stable. We summarize the evolution of Raman gain, random lasing in the non-stationary regime and stationary regime, as shown in the Figure 4.8.
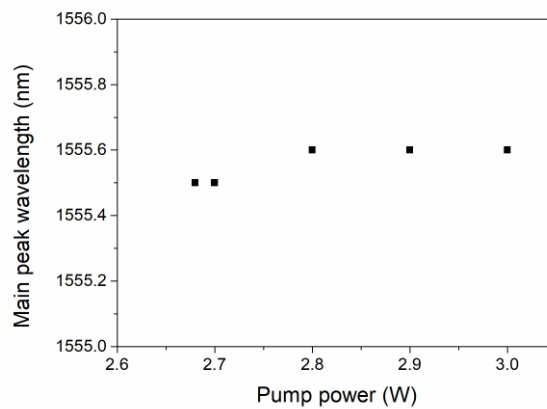
Figure 4. 7 The relationship between of main peak random lasing wavelength and pump power.
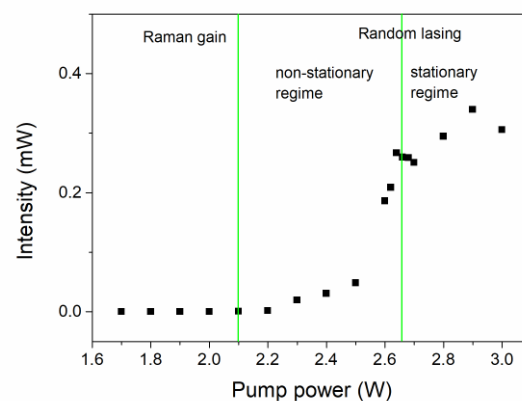
Figure 4. 8 The Raman emission regimes at different pump power.

4.2.3 Random lasing stability

In the above section, we research the random lasing stability in different pump power. In this section, we will research the random lasing stability in different pump time with same pump power. Figure 4.9

60

shows the random lasing spectra at different time at pump power of 2.40 W in the non-stationary regime. It can be seen that there are many random lasing modes and the modes cannot be stabilized, which echoes with the stochastic random lasing emission in the different pump power below 2.68 W. When the pump power increase at 3.00 W, the random lasing emission belong to the stationary regime. Figure 4.10 shows the random lasing spectra at different time at pump power of 3.00 W in the stationary regime. We can see that there are two random lasing modes emission and they can be stabilized in the different pump times. These stabilized random lasing modes can be applied in the optics communications and sensors.
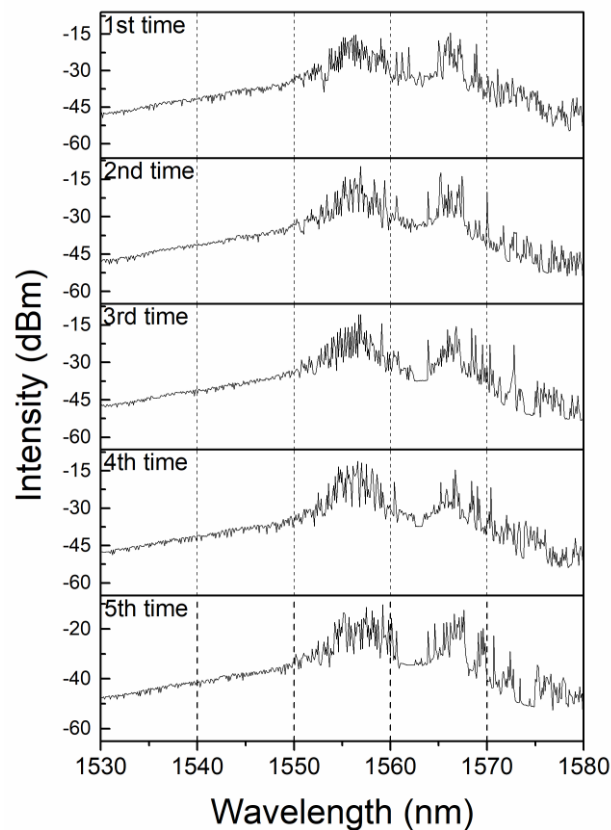
Figure 4. 9 The random lasing emission at pump power of 2.40 W in the different pump times.

4.2.4 Random lasing polarization

In the Chapter 3, we know that 45° TFG have high PER property. In this section, we will research the polarized random fibre lasing using 45° TFG. Figure 4.11 shows the polarized random fibre lasing experimental setup using the polarization scanning technique. The fibre polarizer (P) and fibre polarization controller (PC) have been placed in the front of a 45° TFG. The maximum and minimum

polarized random fibre lasing spectra through 45º TFG can be obtained by rotating the PC. Figure 4.12 shows the measured random fibre lasing PER spectrum by adding 45º TFG with a grating length of 24mm in the Raman distributed feedback system. From the figure, the PER, the difference between the maximum and minimum random fibre lasing emission, has been calculated as 12.02 dB in the 1555.9 nm. This PER with 12.02 dB means that the 45º-TFG couples out 93.7% of s-polarized random fibre lasing from the Raman distributed feedback system.
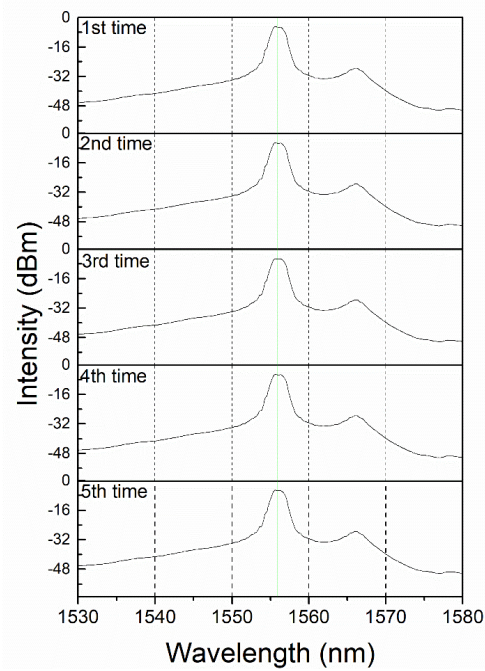
Figure 4. 10 The random lasing emission at pump power of 3.00 W in the different pump times.
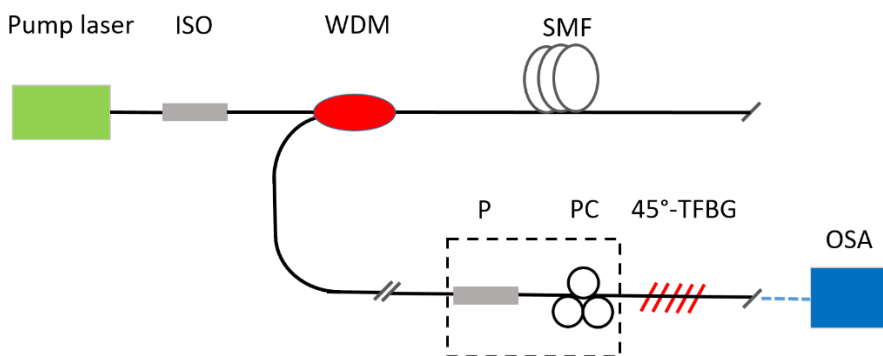
Figure 4. 11 The experimental setup to research polarized RFLs.
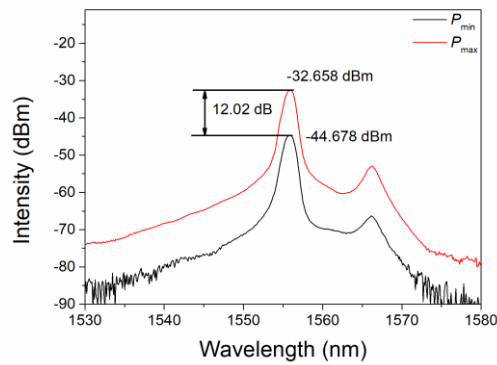
Figure 4. 12 The PER random lasing spectra.

4.3 Erbium-Raman fibre system

4.3.1 Random lasing

In the section, we will research the Erbium-Raman hybrid system to obtain polarized random lasing by add 45° TFG in the hybrid system. The random lasing measured experimental setup has been shown in the Figure 4.13. We add an Erbium doped fibre (EDF) with 2 m length in the front of SMF with length of 11 km. The EDF provides active amplification to decrease the random lasing with the SMF. And the SMF play the same roles with 4.2, presenting Raman gain and distributed feedback.
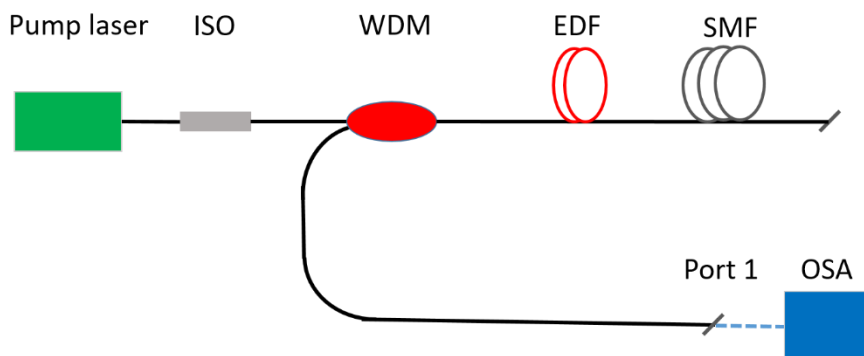
Figure 4. 13 The experimental setup to research RFLs in the Raman distributed feedback system.

When the pump power is low, there are Raman gain and EDF emission from port 1, as shown in the Figure 4.14. In the power of 3.40 W and 3.60 W cases, there are random lasing-like start to emit. When the pump power continues to increase, the random lasing emission is apparent, as shown in the Figure 4.15.
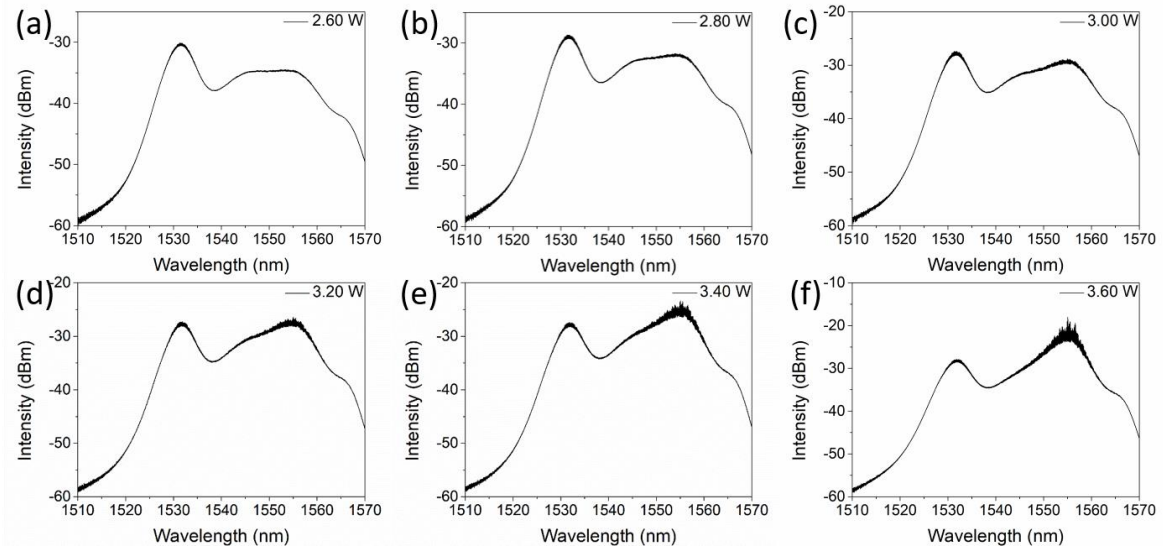
Figure 4. 14 The Raman and Er^{3+}emission spectra for the hybrid system at 14555 nm pumping.
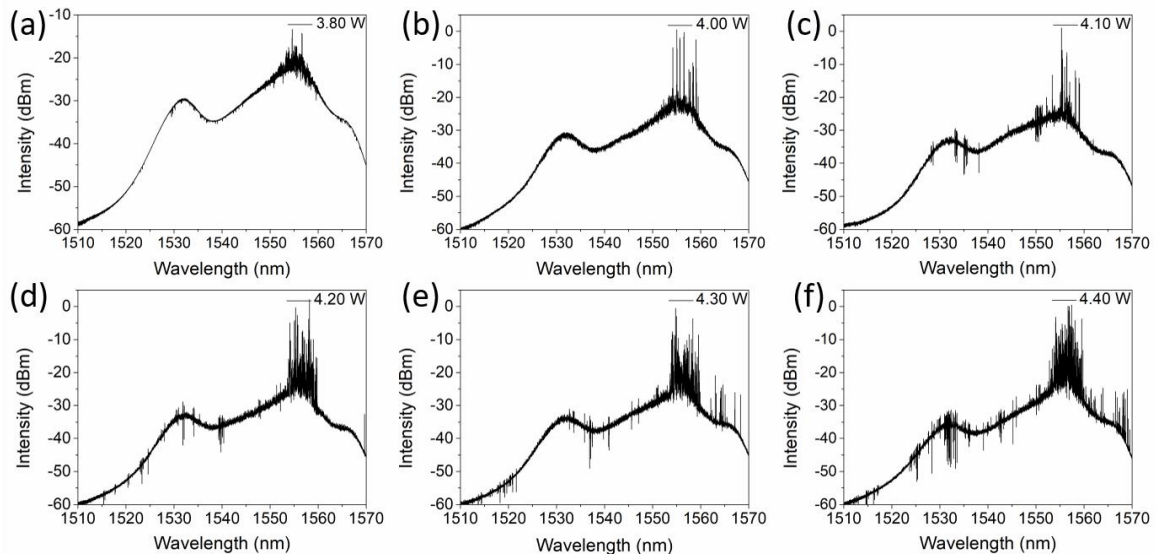
Figure 4. 15 The random lasing emission spectra for the hybrid system at 14555 nm pumping.

From the figure, it can be seen that there are many random lasing modes emission. The random lasing belongs to the non-stationary regime. However, the multi-modes emission basically is from the maximum Raman and Er^{3+} emission. The modes cannot be stabilized with the pump power increasing. Because the maximum power of the Raman pump laser source is below 5 W. Therefore, we cannot observe the stationary random lasing emission in our experiment in the hybrid system. The threshold of hybrid system is higher than that of Raman distributed system, which caused by hybrid system with the short SMF length. Figure 4.16 shows the relationship between the random lasing main peak intensity

and pump power. There is non-linear change in the profile. From the figure, the threshold has been determined as 3.80 W.
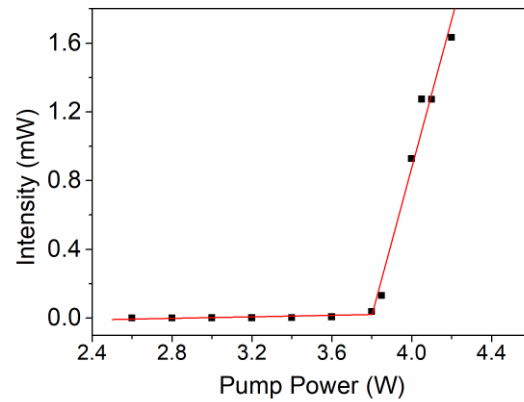
Figure 4. 16 The relationship between of random lasing peak intensity and the pump power in the hybrid system without 45º TFG.

4.3.2 Random lasing stability

In the section, we will research the random lasing emission stability at pump power of 4.40 W in the different pump times, as shown in the Figure 4.17. It can be seen that the random lasing emission modes are around the maximum gain region. The stochastic features are similar with that of Raman system. The random lasing wavelength cannot be fixed. The random lasing emission regime belongs to the non-stationary regime.
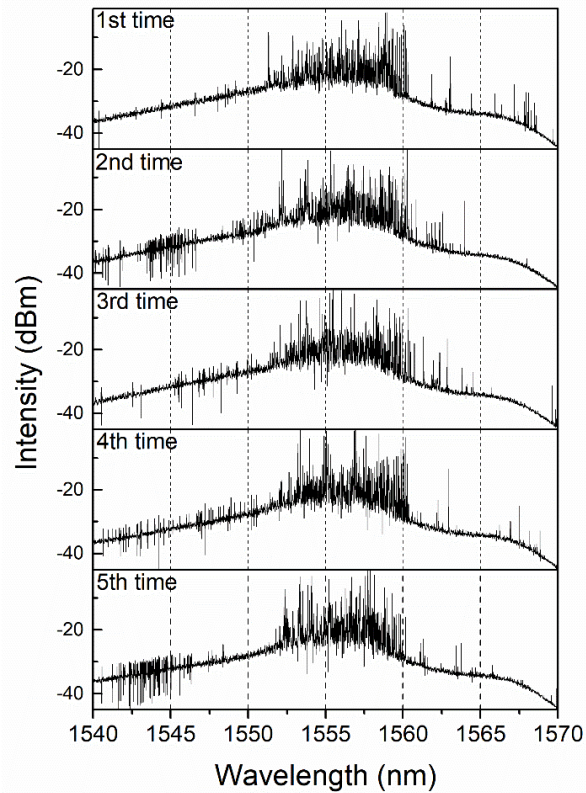
Figure 4. 17 The random lasing emission spectra for the hybrid system at pump power of 4.40 W in different pump times.

4.3.3 Random lasing polarization

The setup of researching random fibre lasing is similar with the Figure 4.11. The EDF has been add in the front of SMF. After the 45° TFG has been added in front of Port 1, we observe different random lasing emission spectra, as shown in the Figure 4.18. When the pump power is below of 1.44 W, there is only Raman and Er^{3+} emission. When the pump power increase over 1.44 W, there occurs random lasing emission. And the random lasing wavelength locates in the 1556.0 nm. The random lasing spectra belongs to stationary regime, which is different from the random emission for the hybrid system without 45° TFG.

The Rayleigh backscattering coefficient of SMF ε is 4.5×10^{-5} km^{-1} [18]. The reflection of 11 km SMF is calculated as 0.05%. The reflection of 45° TFG is measured as 0.09% in 1555.2 nm using fibre circulator. The reflected wavelength is slightly different from the random lasing wavelength, which is due to using different OSA to measure. Therefore, this different reason to obtain stabilized random lasing wavelength in the hybrid system with 45° TFG is caused by the 45° TFG having super-weak

reflection. The 45º TFG forms a weak cavity with the effect of Raman distributed feedback of SMF to boost stabilized random fibre lasing emission. Figure 4.19 shows the relationship of input and output. From the figure, we can obtain the threshold is 1.44 W, which is lower than that of the hybrid system without 45º TFG.
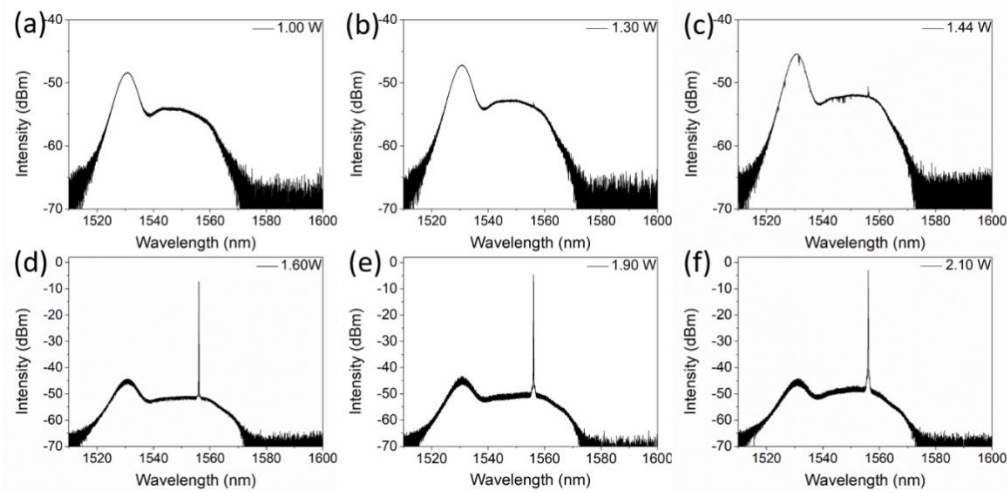
Figure 4. 18 The random lasing emission spectra for the hybrid system with 45º TFG at different pump power.
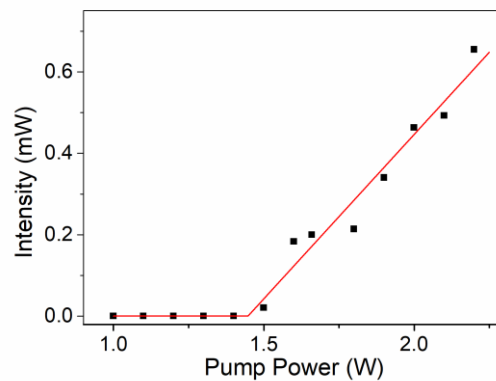
Figure 4. 19 The relationship between of random lasing peak intensity and the pump power in the hybrid system with 45º TFG.

To further research the random lasing stability in the hybrid system with 45º TFG, we measure the random lasing spectra at pump power of 1.60 Win different pump time, as shown in Figure 4.20. In the five spectra, the main peak wavelength is 1555.0 nm. The modes can be stabilized in different pump times. But the intensity changes in the different pump times, which is attributed to the gain perturbation in the EDF and SMF.
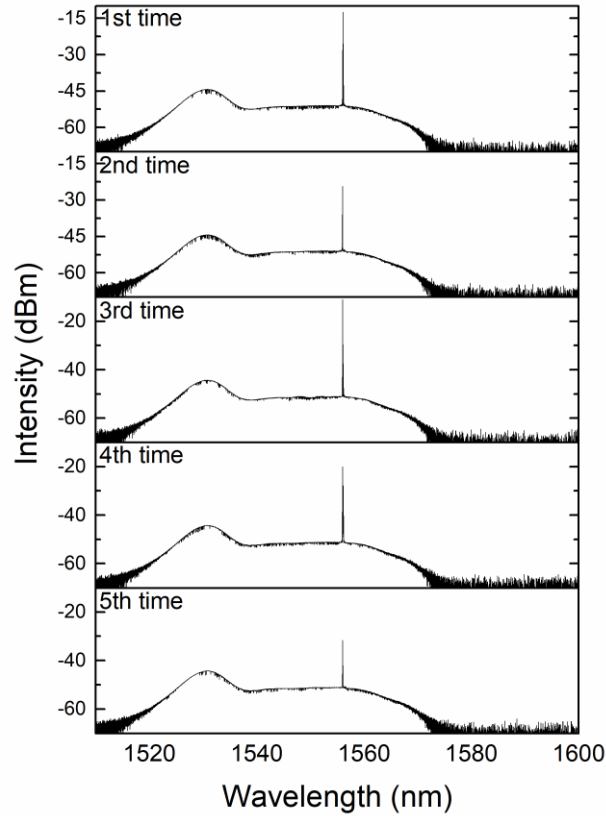
Figure 4. 20 The random lasing emission spectra for the hybrid system with 45º TFG at pump power of 1.60 W in different pump times.

Figure 4.21 shows the measured random fibre lasing PER spectrum in the hybrid system by adding 45º TFG with a grating length of 24mm through rotating PC. From the maximum and minimum random fibre lasing emission spectra, the PER has been calculated as 15.3 dB in the 1556.0 nm. This PER with 15.3 dB means that the 45º-TFG couples out 94.27% of s-polarized random fibre lasing from the hybrid system.
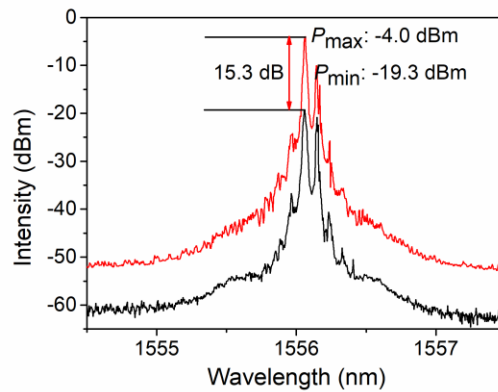
Figure 4. 21 The PER random lasing spectra in the hybrid system with 45º TFG.

4.4 Chapter conclusions

In this chapter, I research random lasing behaviour in the different system: 1) Raman distributed SMF system and 2) EDF and Raman distributed SMF hybrid system. Meanwhile, I research the polarization feature in the two system with 45º TFG.

In the Raman distributed SMF with length of 20.1 km system, there are three kinds of emission with the increase of pump power from 1.70 W to 3.00 W: Raman emission, non-stationary random lasing emission, and stationary random lasing emission. The threshold is measured as 2.10 W. With the 45º TFG effect, the polarized random lasing with PER of 12.02 dB has been obtained.

In the EDF (2 m length) and Raman distributed SMF (11 km length) hybrid system without 45º TFG, there are two kinds of emission with the increase of pump power from 2.60 W to 4.40 W: Raman emission, and non-stationary random lasing. When the 45º TFG has been added in the hybrid system, we observe two kinds of emission in range of pump power of 1.00 W to 2.20 W: Raman and Er^{3+} emission, and stationary random lasing. The weak cavity formed by 45º TFG reflection and SMF distributed feedback boosts the stabilized random fibre lasing emission. The threshold has been determined as 1.44 W. In addition, under the effect of 45º TFG, the polarized random fibre lasing with PER of 15.3 dB has been obtained.

Chapter 5. Conclusions and Future Work

5.1 Conclusions

In this thesis, I have presented my research project on random fibre lasers realised by exploring the spectral and polarization characteristics of fibre gratings, especially the tilted fibre gratings with high PER. As for background review, the thermal and stress sensing applications of FBG, LPG and TFG have also been studied and presented here. In the PER research, I have found the 45° TFGs have high polarized property. Therefore, I have presented the polarized random fibre lasing in the Raman and Raman/EDF system by using 45° TFG, respectively.

The transmissions for small angle TFG, 45° TFG, FBG, and LPG have been researched. In the small angle TFG transmissions including 1°, 3°, and 7°, there are com-like resonance. With the increase of angle, the comb-like wavelength range increases. For the LPG with period 480 μm, there are 11 dips in the range of 1200 nm to 1600 nm. In the PER measurement for small angle TFG and 45° TFG, the 45° TFG has the highest PER value of 14 dB. Also, there are two sets of polarization dependent peaks in the 7° TFG PER spectra corresponding the two polarization statues.

Additionally, the experimental research results of the thermal sensing of different types of fibre grating have been presented. LPG with grating period of 480 μm has the highest thermal sensitivity with 297.1 pm/°C, superior to the FBG, small angle TFG, LPG. Finally, the strain sensing of FBG has been investigated and the strain sensitivity of the FBG is 0.71±0.01 pm/°C.

Based on the polarization property of 45° TFG. The polarized random fibre lasing emission has been demonstrated in the two systems: 1) Raman distributed SMF system; 2) Raman distributed SMF and EDF hybrid system. In the Raman system, the emission successively enters into Raman gain emission, non-stationary random lasing emission and stationary random lasing. With the effect of 45° TFG, the polarized random lasing with PER of 12.02 dB has been obtained. In the Raman distributed SMF and EDF hybrid system, I only observe the Raman gain emission and non-stationary random lasing emission. The stationary random lasing emission cannot be observed because the limit of pump power.

I have researched the random lasing behaviour in two different systems: 1) Raman distributed SMF system and 2) EDF and Raman distributed SMF hybrid system, without and with the polarization property of the 45° TFG. With the effect of 45° TFG in the hybrid system, we observed different random

lasing emission phenomenon. There is stationary random lasing emission in the low pump power of 1.44 W. This is caused by the super weak cavity formed by 45º TFG reflection and SMF distributed feedback. In addition, the polarized random fibre lasing with PER of 15.3 dB has been obtained in the hybrid system with 45º TFG.

5.2 The future works

5.2.1 Comb-like random fibre lasing

In the Chapter 2, the small angle TFG exhibits the comb-like transmission spectra. And in the chapter 3, we know the super weak reflection can form weak cavity with Raman distributed system to boost stabilized random lasing emission. Therefore, the small angle TFG, especially 7º TFG, can be integrated in the Raman or Raman/EDF system to obtain comb random fibre lasing in the wide wavelength range. The weak reflection of 7º TFG can form a weak cavity with the Raman distributed system to boost stabilized random fibre lasing emission.

5.2.2 Polarized comb-like random fibre lasing.

In the chapter 4, the polarized fibre random lasing has been obtained using 45º TFG. It is very important in the optical communications and sensors. And the 7º TFG has better feature to obtain comb-like lasers. Therefore, it is impossible to obtain polarized comb-like random fibre lasing emission to integrate 45º TFG and 7º TFG in the SMF system. Figure 5.1 shows the experimental setup.
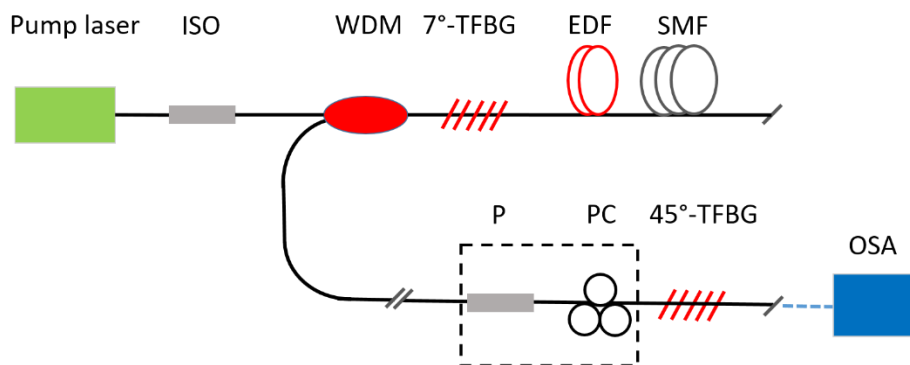
Figure 5. 1 The schematic of polarized comb-like random fibre lasing using hybrid 45° TFG and 7º TFG.

Publications

Journal paper: # Co-first author, *corresponding author

1. Z. Hu (*#), Rui Ma (#), **X. Zhang** (#), Z. Sun, X. Liu, Jun Liu, K. Xie (*), L. Zhang, Weak feedback assisted random fiber laser from 45°-tilted fiber Bragg grating, Opt. Express, 2019, 27(3), 3255-3263.

2. X. Chen (#), K. Xie (#), **X. Zhang** (#), Z. Xie, J. Ma, J. Wen, J. Chen, J. Zhang, X. Cheng, and Z. Hu (*), Polymer-fiber random lasers based on pumping radiation effect, Physica Scripta, 2019, accepted.

3. H. Lu (*), C. Wei, Q. Zhang, M. Xu, Y. Ding, G. Zhang, J. Zhu, K. Xie, **X. Zhang**, Z. Hu (*), and L. Qiu, Wide tunable laser based on electrically regulated bandwidth broadening in polymer-stabilized cholesteric liquid crystal, Photonics Res., 2019, 7(2), 137-143.

4. Z. Zhang, L. Yin, J. Xia, K. Xie, G. Zou, **X. Zhang**, Z. Hu (*), and Q. Zhang (*), Near-field scattering enhancement of perylene based aggregates for random lasing, Chinese J. Chem. Phys., 2019, DOI:10.1063/1674-0068/cjcp1807167.

5. J. Xia (#), J. He(#), K. Xie(#), **X. Zhang**, L. Hu, Y. Li, X. Chen, J. Ma, J. Wen, J. Chen, Q. Pan, J. Zhang, I. D. Vatnik, D. Churkin, and Z. Hu(*), Replica Symmetry Breaking in FRET-assisted random laser based on Eelectrospun polymer fiber, Annalen der Physik, 2019, DOI: 10.1002/andp.201900066.

References

[1] Letokhov, V. S. "Stimulated emission of an ensemble of scattering particles with negative absorption," Sov. Phys.–JETP, 5(8), 212-215, 1967.

[2] Letokhov, V. S. "Quantum statistics of multiple- mode emission of an atomic ensemble," Sov. Phys.–JETP, 26(6), 1246-1251, 1968.

[3] Cao, H.; Zhao, Y. G.; Ho, S. T.; Seelig, E. W.; Wang, Q. H.; and Chang, R. P. H. "Random laser action in semiconductor powder," Phys. Rev. Lett., 82(11), 2278-2281, 1999.

[4] Wiersma, D. S.; and Lagendijk, A. "Light diffusion with gain and random lasers," Phys. Rev. E, 54(4), 4256-4265, 1997.

[5] Lawandy, N. M.; Balachandran, R. M.; Gomes, A. S. L.; and Sauvain, E. "Laser action in strongly scattering media," Nature, 368, 436-438, 1994.

[6] Frolov, S. V.; Vardeny, Z. V.; Yoshino, K.; Zakhidov, A.; and Baughman, R. H. "Stimulated emission in high-gain organic media," Phys. Rev. B, 59(8), R5284-R5287, 1999.

[7] Frolov, S. V.; Vardeny, Z. V.; Zakhidov, A. A.; and Baughman, R. H. "Laser-like emission in opal photonic crystals," Opt. Commun., 162(4-6), 241-246, 1999.

[8] Polson, R. C.; Chipouline, A.; and Vardeny, Z. V. "Random lasing in π-conjugated films and infiltrated opals," Adv. Mater., 13(10), 760-764, 2001.

[9] Cao, H. "Lasing in random media," Wave Random Media, 13, R1-R39, 2003.

[10] Cao, H.; Zhao, Y. G.; Ong, H. C.; Ho, S. T.; Dai, J. Y.; Wu, J. Y.; and Chang, R. P. H. "Ultraviolet lasing in resonators formed by scattering in semiconductor polycrystalline films," Appl. Phys. Lett., 73(25), 3656-3658, 1998.

[11] Chen, Y.; Herrnsdorf, J.; Guilhabert, B.; Zhang, Y.; Watson, I. M.; Gu, E.; Laurand, N.; and Dawson, M. D. "Colloidal quantum dot random laser," Opt. Express, 19(4), 2996-3003, 2011.

[12] Yao, Y.; Yang, Z.-P.; Hwang, J.-M.; Su, H.-C.; Haung, J.-Y.; Lin, T.-N.; Shen, J.-L.; Lee, M.-H.; Tsai, M.-T.; and Lee, Y.-J. "Coherent and polarized random laser emissions from colloidal CdSe/ZnS quantum dots plasmonically coupled to ellipsoidal Ag nanoparticles," Adv. Opt. Mater, 5 (3), 1600746, 2017.

[13] Redding, B.; Choma, M. A.; and Cao, H. "Speckle-free laser imaging using random laser illumination," Nature Phys., 6, 355-359, 2012.

[14] de Matos, C. J. S.; Menezes, L. de S.; Brito-Silva, A. M.; Gámez, M. A. M.; Gomes, A. S. L.; and de Araújo, C. B. "Random fiber laser," Phys. Rev. Lett., 99(15), 153903, 2007.

[15] Hu, Z.; Zheng, H.; Wang, L.; Tian, X.; Wang, T.; Zhang, Q.; Zou, G.; Chen, Y.; and Zhang, Q. "Random fiber laser of POSS solution-filled hollow optical fiber by end pumping," Opt. Commun, 285(19), 3967-3970, 2012.

[16] Hu, Z.; Zhang, Q.; Miao, B.; Fu, Q.; Zou, G.; Chen, Y.; Luo, Y.; Zhang, D.; Wang, P.; Ming, H.; and Zhang, Q. "Coherent random fiber laser based on nanoparticles scattering in the extremely weakly scattering regime," Phys. Rev. Lett., 109(25), 253901, 2012.

[17] Hu, Z.; Miao, B.; Wang, T.; Fu, Q.; Zhang, D.; Ming, H.; and Zhang, Q. "Disordered microstructure polymer optical fiber for stabilized coherent random fiber laser," Opt. Lett., 38(22), 4644-4647, 2013.

[18] Turitsyn, K.; Babin, S. A.; EI-Taher, A. E.; Harper, P.; Churkin, D. V.; Kablukov, S. I.; Ania-Castañón, J. D.; Karalekas, V.; and Podivilov, E. V. "Random distributed feedback fibre laser," Nat. Photonics, 4, 231-235, 2010.

[19] Pang, M.; Xie, S.; Bao, X.; Zhou, D.-P.; Lu, Y.; and Chen, L. "Rayleigh scattering-assisted narrow linewidth Brillouin lasing in cascaded fiber," Opt. Lett., 37(15), 3129-3131, 2012.

[20] Knitter, S.; Kues, M.; and Fallnich, C. "Emission polarization of random lasers in organic dye solutions," Opt. Lett., 37(17), 3621-3623, 2012.

[21] Wang, C.; and Liu, J. "Polarization dependence of lasing modes in two-dimensional random lasers," Phys. Lett. A, 353(1-2), 269-272, 2006.

[22] Ma, R.; Rao, Y.; Zhang, W.; Hu, B. "Multimode random fiber laser for speckle-free imaging," IEEE J. Sel. Top. Quant. Electron. 25 (1), 1-6, 2019.

[23] Zhou, K.; Simpson, G.; Chen, X.; Zhang, L.; and Bennion, I. "High extinction ratio in-fiber polarizers based on 45° tilted fiber Bragg gratings," Opt. Lett., 30(11), 1285-1287, 2005.

[24] Ambartsumyan, R. V.; Kryukov, P. G.; Letokhov, V. S. "Dynamics of emission line narrowing for a laser with nonresonant," Sov. Phys.–JETP 1967, 24(6), 1129-1134.

[25] Ambartsumyan, R. V.; Kryukov, P. G.; Letokhov, V. S.; Matveets, Y. A. "Statistical emission properties of a nonresonant feedback laser," Sov. Phys.–JETP 1968, 26(6), 1109-1114.

[26] Wiersma, D. S. "The physics and applications of random lasers," Nature Phys., 4, 359-367, 2008.

[27] Bravo-Abad, J.; and Soljacic, M. "A unified picture of laser physics," Science, 320, 623-624, 2008.

[28] Mujumdar, S.; Ricci, M.; Torre, R.; and Wiersma, D. S. "Amplified extended modes in random lasers," Phys. Rev. Lett., 93(5), 053903, 2004.

[29] Meng, X.; Fujita, K.; Murai, S.; and Tanaka K. "Coherent random lasers in weakly scattering polymer films containing silver nanoparticles," Phys. Rev. A, 79(5), 053817, 2009.

[30] Costela, A.; Garcia-Moreno, I.; Cerdan, L.; Martin, V.; Garcia, O.; and Sastre, R. "Dye-doped POSS solutions: random nanomaterials for laser emission," Adv. Mater., 21(41), 4163-4166, 2009.

[31] Tulek, A.; Polson, R. C.; and Vardeny, Z. V. "Naturally occurring resonators in random lasing of π-conjugated polymer films," Nature Phys., 6(4), 303-310, 2010.

[32] Zhao, X.; Wu, Z.; Ning, S.; Liang, S.; Wang, D.; and Hou, X. "Random lasing from granular surface of waveguide with blends of PS and PMMA," Opt. Express, 19(17), 16126-16131, 2011.

[33] Hands, P. J. W.; Gardiner, D. J.; Morris, S. M.; Mowatt, C.; Wilkinson, T. D. and Colesb, H. J. "Band-edge and random lasing in paintable liquid crystal emulsions," Appl. Phys. Lett., 98(14), 141102, 2011.

[34] Strangi, G.; Ferjani, S.; Barna, V.; De Luca, A.; Versace, C.; Scaramuzza, N.; and Bartolino, R. "Random lasing and weak localization of light in dye-doped nematic liquid crystals," Opt. Express, 14(17), 7737-7744, 2006.

[35] Polson, R. C.; Chipouline, A.; and Vardeny, Z. V. "Random lasing in π-conjugated films and infiltrated opals," Adv. Mater. 13(10), 760-764, 2001.

[36] Lisinetskii, V.; Ryabchun, A.; Bobrovsky, A.; and Schrader, S. "Photochromic composite for random lasing based on porous polypropylene infiltrated with azobenzene-containing liquid crystalline mixture," ACS Appl. Mater. Interfaces, 7(48), 26595-26602, 2015.

[37] Yashchuk, V. P.; Prygodiuk, O.; Koreniuk, V.; Tikhonov, E.; Bezrodny, V. "Random lasing in porous scattering medium," Appl. Phys. B, 92(4), 593-597, 2008.

[38] Prasad, B. R.; Ramachandran, H.; Sood, A. K.; Subramanian, C. K.; and Kumar, N. "Lasing in active, sub-mean-free path-sized systems with dense, random, weak scatterers," Appl. Opt., 36(30), 7718-7724, 1997.

[39] Wu, X.; Fang, W.; Yamilov, A.; Chabanov, A. A.; Asatryan, A. A.; Botten, L. C.; and Cao, H. "Random lasing in weakly scattering systems," Phys. Rev. A, 74(5), 053812, 2006.

[40] Ferjani, S.; Barna, V.; De Luca, A.; Versace, C.; Scaramuzza, N.; Bartolino, R.; and Strangi, G. "Thermal behavior of random lasing in dye doped nematic liquid crystals," Appl. Phys. Lett., 89(12), 121109, 2006.

[41] Lu, H.; Xing, J.; Wei, C.; Xia, J.; Sha, J.; Ding, Y.; Zhang, G.; Xie, K.; Qiu, L.; and Hu, Z. "Band gap tailored random laser," Photonics Res., 6(5), 390-395, 2018.

[42] Tulek, A.; and Vardeny, Z. V. "Studies of random laser action in π-conjugated polymers," J. Opt., 12(2) 024008, 2010.

[43] Deng, C.; He, Q.; He, C.; Shi, L.; Cheng, J.; and Lin, T. "Conjugated polymer-titania nanoparticle hybrid films: random lasing action and ultrasensitive detection of explosive vapors," J. Phys. Chem. B, 114(13), 4725-4730, 2010.

[44] Yoshino, K.; Tatsuhara, S.; Kawagishi Y.; Ozaki, M.; Zakhidov, A. A.; Vardeny, Z. V. Amplified spontaneous emission and lasing in conducting polymers and fluorescent dyes in opals as photonic crystals, Appl. Phys. Lett., 74(18), 2590-2592, 1999.

[45] Hu, Z.; Liang, Y.; Xie, K.; Gao, P.; Zhang, D.; Jiang, H.; Shi, F.; Yin, L.; Gao, J.; Ming, H.; and Zhang, Q. "Gold nanoparticles-based plasmonic random fiber laser," J. Opt., 17(3), 035001, 2015.

[46] Zhang, L.; Xu, Y.; Gao, S.; Saxena, B.; Chen, L.; and Bao, X. "Power scaling of linearly polarized random fiber laser," IEEE J. Sel. Top. Quant. 24, 0900308, 2018.

[47] Sheeba, M.; Thomas, K. J.; Rajesh, M.; Nampoori, V. P. N.; Vallabhan, C. P. G.; and Radhakrishnan, P. "Multimode laser emission from dye doped polymer optical fiber," Appl. Opt. 46(33), 8089-8094, 2007.

[48] Liang, H.; Zhang, Q. J.; Zheng, Z. Q.; Ming, H.; Li, Z. C.; Xu, J.; Chen, B.; and Zhao, H. "Optical amplification of Eu(DBM)$_3$Phen-doped polymer optical fiber," Opt. Lett. 29(5), 477-479, 2004.

[49] Zubia, J.; and Arrue, J. "Plastic optical fibers: an introduction to their technological processes and applications," Opt. Fiber Technol. 7(2), 101-140, 2001.

[50] Quandt, B. M.; Pfister, M. S.; Lübben, J. F.; Spano, F.; Rossi, R. M.; Bona, G.-L.; and Boesel, L. F. "POF-yarn weaves: controlling the light outcoupling of wearable phototherapy devices," Biomed. Opt. Express 8(10), 4316-4330, 2017.

[51] Abaie, B.; Mobini, E.; Karbasi, S.; Hawkins, T.; Ballato, J.; and Mafi, A. "Random lasing in an Anderson localizing optical fiber," Light: Sci. & Appl., 6, e17041, 2017.

[52] Hu, Z.; Gao, P.; Xie, K.; Liang, Y.; and Jiang, H. "Wavelength control of random polymer fiber laser based on adaptive disorder," Opt. Lett., 39(24), 6911-6914, 2014.

[53] He, J.; Chan, W. K. E.; Cheng, X.; Tse, M. L.V.; Lu, C.; Wai, P. K. A.; Savovic, S.; Tam, H.-Y. "Experimental and theoretical investigation of the polymer optical fiber random laser with resonant feedback," Adv. Opt. Mater., 6(7), 1701187, 2018.

[54] Knitter, S.; Kues, M.; Haidl, M.; and Fallnich, C. "Linearly polarized emission from random lasers with anisotropically amplifying media," Opt. Express, 21(25), 31591-31603, 2013.

[55] Ye, L.; Li, F.; Lu, C.; Cheng, Z.; Hu, G.; Lu, Y.; and Cui Y. "The controllable intensity and polarization degree of random laser from sheared dye-doped polymer-dispersed liquid crystal," Nanophotonics, 7(2), 473-478, 2018.

[56] Ni, Y. X.; Gao, L.; Miroshnichenko, A. E.; and Qiu, C. W. "Controlling light scattering and polarization by spherical particles with radial anisotropy," Opt. Express, 21(7), 8091-8100, 2013.

[57] Liu, J. S.; Xiong, Z.; and Chun, W. "Theoretical investigation on polarization-dependent laser action in two-dimensional random media," J. Opt. A: Pure Appl. Opt., 9(7), 658-663, 2007.

[58] Yao, F.; Bian, H.; Pei, Y.; Hou, C.; and Sun, X. "Behaviors of random laser in dye-doped nematic liquid crystals," Opt. Commun., 359, 15-19, 2016.

[59] Xiao, S.; Song, Q.; Wang, F.; Liu, L.; Liu, J.; and Xu, L. "Switchable random laser from dye-doped polymer dispersed liquid crystal waveguides," IEEE J. Quantum Elect., 43(5-6), 407-410, 2007.

[60] Leong, E. S. P.; Yu, S. F.; Abiyasa, A. P.; and Lau, S. P. "Polarization characteristics of ZnO rib waveguide random lasers," Appl. Phys. Lett., 88(9), 091116, 2006.

[61] Wu, H.; Wang, Z.; Churkin, D. V.; Vatnik, I. D.; Fan, M. Q.; and Rao, Y. "Random distributed feedback Raman fiber laser with polarized pumping," Laser Phys. Lett., 12(1), 015101, 2015.

[62] Du, X.; Zhang, H.; Wang, X.; Zhou, P.; and Liu, Z. "Investigation on random distributed feedback Raman fiber laser with linear polarized output," Photon. Res., 3(2), 28-31, 2015.

[63] Zlobina, E. A.; Kablukov, S. I.; and Babin, S. A. "Linearly polarized random fiber laser with ultimate efficiency," Opt. Lett., 40(17), 4074-4077, 2015.

[64] Xu, J.; Huang, L.; Jiang, M.; Ye, J.; Ma, P.; Leng, J.; Wu, J.; Zhang, H.; and Zhou, P. "Near-diffraction-limited linearly polarized narrow-linewidth random fiber laser with record kilowatt output," Photon. Res., 5(4), 350-354, 2017.

[65] Ye, J.; Xu, J.; Song, J.; Xu, H.; Wu, H.; Zhang, H.; Leng, J.; and Zhou, P. "Power scalability of linearly polarized random fiber laser through polarization-rotation-based Raman gain manipulation," Opt. Express, 26(18), 22894-22903, 2018.

[66] Yao, B.; Rao, Y.; Wang, Z.; Wu, Y.; Zhou, J.; Wu, H.; Fan, M.; Cao, X.; Zhang, W.; Chen, Y.; Li, Y.; Churkin, D.; Turitsyn, S.; and Wong, C. W. "Graphene based widely-tunable and singly-polarized pulse generation with random fiber lasers," Sci. Rep., 5, 18526, 2015.

[67] Zhang, L.; Xu, Y.; Gao, S.; Saxena, B.; Chen, L.; and Bao, X. "Linearly polarized low-noise Brillouin random fiber laser," Opt. Lett., 42(4), 739-742, 2017.

[68] Zhang, L.; Wang, C.; Li, Z.; Xu, Y.; Saxena, B.; Gao, S.; Chen, L.; and Bao, X. "High-efficiency Brillouin random fiber laser using all-polarization maintaining ring cavity," Opt. Express, 25(10), 11306-11314, 2017.

[69] Hu, Z.; Liang, Y.; Qian, X.; Gao, P.; Xie, K.; and Jiang, H. "Polarized random laser emission from an oriented disorder polymer optical fiber," Opt. Lett., 41(11), 2584-2587, 2016.

[70] Hill, K. O.; Fujii, Y.; Johnson, D. C.; and Kawasaki, B. S. "Photosensitivity in optical fiber waveguides-application to reflection filter fabrication." Appl. Phys. Lett., 32(10), 647-649, 1978.

[71] Lam, D. K. W.; and Garside, B. K. "Characterization of single-mode optical fiber filters," Appl. Opt., 20(3), 440-445, 1981.

[72] Meltz, G.; Morey, W. W.; and Glenn, W. H. "Formation of Bragg gratings in optical fibers by a transverse holographic method," Opt. Lett., 14(15), 823-825, 1989.

[73] Meltz, G.; Morey, W. W.; Glenn, W. H. "In-fibre Bragg grating tap," Optical Fibre Communications, San Francisco, California, USA, OSA Technical Digest Series 1, TUG1, 1990.

[74] Hill, K. O.; Malo, B.; Bilodeau, F.; Johnson, D. C.; and Albert, J. "Bragging gratings fabricated in monomode photosensitive optical fibre by UV exposure through a phase mask," Appl. Phys. Lett., 62(10), 1035-1037, 1993.

[75] Anderson, D. Z.; Mizrahi, V.; Erdogan, T.; and White, A. "Production of in-fibre gratings using a diffractive optical element," Electron. Lett., 29(6), 566-568, 1993.

[76] Armitage, J. R. "Fibre Bragg reflectors written at 262 nm using a frequency quadrupled diode-pumped Nd^{3+}:YLF laser," Electron. Lett., 29(13), 1181-1183, 1993.

[77] Hill, K. O.; Bilodeau, F.; Malo, B.; Kitagawa, T.; Thériault, S.; Johnson, D. C.; Albert, J.; and Takiguchi, K. "Chirped in-fiber Bragg gratings for compensation of optical-fiber dispersion," Opt. Lett., 19(17), 1314-1316, 1994.

[78] Vengsarkar, A. M.; Lemaire, P. J.; Judkins, J. B.; Bhatia, V.; Erdogan, T.; and Sipe, J. E. "Long-period fiber gratings as band-rejection filters," J. Lightwave Technol., 14(1), 58-65, 1996.

[79] Westbrook, P. S.; Strasser, T. A.; Erdogan, T. "In-line polarimeter using blazed fibre gratings," IEEE Photon. Technol. Lett., 12(10), 1352-1354, 2000.

[80] Zhou, K.; Zhang, L.; Chen, X.; and Bennion, I. "Optic sensors of high refractive-index responsivity and low thermal cross sensitivity that use fiber Bragg gratings of >80° tilted structures," Opt. Lett., 31(9), 1193-1195, 2006.

[81] Hill, K. O.; Malo, B.; Bilodeau, F.; Johnson, D. C.; Morse, T. F.; Kilian, A.; Reinhart, L.; and Oh, K. "Photosensitivity in Eu^{2+}:Al_2O_3-doped-core fiber: preliminary results and application to mode converters," Optical Fiber Communication, Vol. 4, paper PD3, OSA Technical Digest Series, 1991.

[82] Taunay, T.; Bernage, P.; Douay, M.; Xié, W. X.; Martinelli, G.; Niay, P.; Bayon, J. F.; Delevaque, E.; and Poignant, H. "Ultraviolet-enhanced photosensitivity in cerium-doped aluminosilicate fibers and glasses through high-pressure hydrogen loading," J. Opt. Soc. Am. B, 14(4), 912-925, 1997.

[83] Malo, B.; Albert, J.; Bilodeau, F.; Kitagawa, T.; Johnson, D. C.; Hill, K. O.; Hattori, K.; Hibino, Y.; and S. Gujrathi, "Photosensitivity in phosphorus-doped silica glass and optical waveguides," Appl. Phys. Lett., 65(4), 394-396, 1994.

[84] Bilodeau, F.; Johnson, D. C.; Malo, B.; Vineberg, K. A.; Hill, K. O.; Morse, T. F.; Kilian, A.; and Reinhart, L. "Ultraviolet-light photosensitivity in Er^{3+}-Ge-doped optical fiber," Opt. Lett., 15(20), 1138-1140, 1990.

[85] Hand, D. P. and Russell, P. S. J. "Photoinduced refractive-index changes in germanosilicate fibers," Opt. Lett., 15(2), 102-104, 1990.

[86] Fiori, C.; and Devine, R. A. B. "Evidence for a wide continuum of polymorphs in α-SiO2," Phys. Rev. B, 33(4), 2972-2974, 1986.

[87] Wong, D.; Poole, S. B.; and Sceats, M. G. "Stress-birefringence reduction in elliptical-core fibers under ultraviolet irradiation," Opt. Lett., 17(24), 1773-1775, 1992.

[88] Lawandy, N. "Light induced transport and delocalization in transparent amorphous systems," Opt. commun., 74(3-4), 180-184, 1989.

[89] Williams, D. L.; Ainslie, B. J.; Kashyap, R.; Maxwell, G. D.; Armitage, J. R.; Campbell, R. J.; and Wyatt, R. "Photosensitive index changes in germania-doped silica glass fibers and waveguides," Proc. SPIE, 2044, 55-68, 1993.

[90] Attard, A. E. "Fermi level shift in $Bi_{12}SiO_{20}$ via photon-induced trap level occupation," J. Appl. Phys., 71(2), 933-937, 1992.

[91] Miotello, A.; and Kelly, R. "Laser irradiation effects in Si^+-implanted SiO_2," Nucl. Instrum. Meth. B, 65(1-4), 217-222, 1992.

[92] Yuen, M. J. "Ultraviolet absorption studies of germanium silicate glasses," Appl. Opt., 21(1), 136-140, 1982.

[93] Russell, P.S., Hand, D. P.; Chow, Y. T.; Poyntz-Wright, L. J. "Optically-induced creation, transformation and organization of defects and color-centers in optical fibers," Proc. SPIE 1516, International Workshop on Photoinduced Self-Organization Effects in Optical Fiber, 1516, 47-54, 1991.

[94] Limberger, H. G.; Fonjallaz, P. Y.; Salathe, R. P.; Cochet, F. "Compaction- and photoelastic-induced index changes in fiber Bragg gratings," Appl. Phys. Lett., 68(22), 3069-3071, 1996.

[95] Patrick, H.; and Gilbert, S. L. "Growth of Bragg gratings produced by continuous-wave ultraviolet-light in optical-fiber," Opt. Lett., 18(18), 1484-1486, 1993.

[96] Williams, D. L.; Davey, S. T.; Kashyap, R.; Armitage, J. R.; Ainslie, B. J. "Direct observation of UV induced bleaching of 240 nm absorption-band in photosensitive germanosilicate glass fibers," Electron. Lett., 28(4), 369-371, 1992.

[97] Dong, L.; Archambault, J. L.; Reekie, L.; Russell, P. S. J.; and Payne, D. N. "Photoinduced absorption change in germanosilicate preforms: evidence for the color-center model of photosensitivity," Appl. Opt., 34(18), 3436-3440, 1995.

[98] Leconte, B.; Xie, W.; Douay, M.; Bernage, P.; Niay, P.; Bayon, F. J.; Delevaque, E.; and Poignant H. "Analysis of color-center-related contribution to Bragg grating formation in $Ge:SiO_2$ fiber based on a local Kramers-Kronig transformation of excess loss spectra," Appl. Opt., 36(24), 5923-5930, 1997.

[99] Rothschild, M.; Ehrlich, D. J.; and Shaver, D. C. "Effects of excimer laser irradiation on the transmission, index of refraction, and density of ultraviolet grade fused silica," Appl. Phys. Lett., 55(13), 1276-1278, 1989.

[100] Allan, D. C.; Smith, C.; Borrelli, N. F.; and Seward, T. P. "193-nm excimer-laser-induced densification of fused silica," Opt. Lett., 21(24), 1960-1962, 1996.

[101] Douay, M.; Xie, W. X.; Taunay, T.; Bernage, P.; Niay, P.; Cordier, P.; Poumellec, B.; Dong, L.; Bayon, J. F.; Poignant, H.; Delevaque, E. "Densification involved in the UV-based photosensitivity of silica glasses and optical fibers," J. Lightwave Technol., 15(8), 1329-1342, 1997.

[102] Sceats, M. G.; Atkins, G. R.; and Poole, S. B. "Photolytic index changes in optical fibers," Annu. Rev. Mater. Sci., 23, 381-410, 1993.

[103] Erdogan, T.; Mizrahi, V.; Lemaire, P. J.; and Monroe, D. "Decay of ultraviolet-induced fiber Bragg gratings," J. Appl. Phys., 76(1), 73-80, 1994.

[104] Patrick, H.; and Gilbert, S. L. "Annealing of Bragg gratings in hydrogen-loaded optical fiber," J. Appl. Phys., 78(5), 2940-2945, 1995.

[105] Baker, S. R.; Rourke, H. N.; Baker, V.; and Goodchild, D. "Thermal decay of fiber Bragg gratings written in boron and germanium codoped silica fiber," J. Lightwave Technol., 15(8), 1470-1477, 1997.

[106] Zhou, K.; Zhang, L.; Chen, X.; Bennion, I. "Low thermal sensitivity grating devices based on Ex-45° tilting structure capable of forward-propagating cladding modes coupling," J. Lightwave Technol., 24(12), 5087-5094, 2006.

[107] Shu, X.; Zhang, L.; and Bennion, I. "Sensitivity characteristics of long-period fiber gratings," J. Lightwave Technol., 20(2), 255-266, 2002.

[108] Young, M. "Optics and lasers: including fibers and optical waveguides," Vol. 5, Springer Science & Business Media, 2000.

[109] Agilent Technologies, "Polarization dependent loss measurement of passive optical components application note," 5988-1232EN, 2001.

[110] Shu, X.; Allsop, T.; Gwandu, B.; Zhang, L.; and Bennion, I. "Room-temperature operation of widely tunable loss filter," Electron. Lett., 37(4), 216-218, 2001.

[111] MacDougall, T. W.; Pilevar, S.; Haggans, C. W.; and Jackson, M. A. "Generalized expression for the growth of long period gratings," IEEE Photon. Technol. Lett., 10(10), 1449–1451, 1998.

[112] Rottwitt, K.; Bromage, J.; Stentz, A. J.; Leng, L.; Lines, M. E.; Smith, H. "Scaling of the Raman gain coefficient: applications to germanosilicate fibers," J. Lightwave Technol., 21(7), 1652-1662, 2003.

[113] Churkin, D. V.; Babin, S. A.; El-Taher, A. E.; Harper, P.; Kablukov, S. I.; Karalekas, V.; Ania-Castañón, J. D.; Podivilov, E. V.; and Turitsyn, S. K. "Raman fiber lasers with a random distributed feedback based on Rayleigh scattering," Phys. Rev. A, 82(3), 033828, 2010.

[114] Turitsyn, S. K.; Babin, S. A.; Churkin, D. V.; Vatnik, I. D.; Nikulin, M.; Podivilov, E. V. "Random distributed feedback fibre lasers," Phys. Rep., 542(2), 133-193, 2014.